

College of Saint Benedict and Saint John's University

DigitalCommons@CSB/SJU

Honors Theses, 1963-2015

Honors Program

1991

The Quantum Magneto Effect of Bismuth

Omar Kerem Durdag

College of Saint Benedict/Saint John's University

Follow this and additional works at: https://digitalcommons.csbsju.edu/honors_theses



Part of the [Physics Commons](#)

Recommended Citation

Durdag, Omar Kerem, "The Quantum Magneto Effect of Bismuth" (1991). *Honors Theses, 1963-2015*. 770.
https://digitalcommons.csbsju.edu/honors_theses/770

Available by permission of the author. Reproduction or retransmission of this material in any form is prohibited without expressed written permission of the author.

THE QUANTUM MAGNETO EFFECT IN BISMUTH

The Honors Program
College of St. Benedict/St. John's University

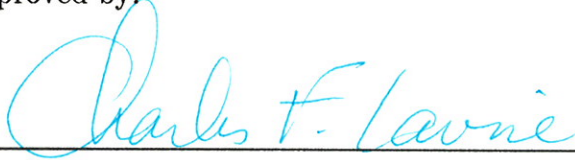
In Partial Fulfillment
of the Requirements for the Distinction of "All College Honors"
and the Degree Bachelor of Science
In the Department of Physics

by
Ömer Kerem Durdağ
May, 1991

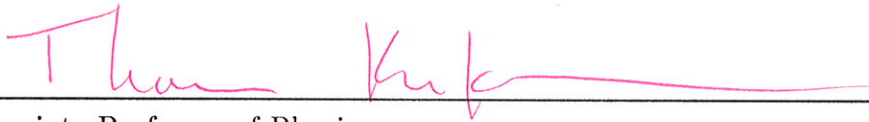
THESIS APPROVAL PAGE

PROJECT TITLE: THE QUANTUM MAGNETO EFFECT OF BISMUTH

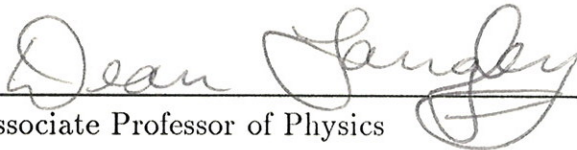
Approved by:



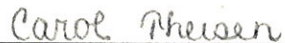
Associate Professor of Physics



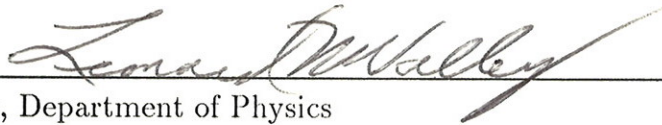
Associate Professor of Physics



Associate Professor of Physics



Assistant Professor of Physics



Chair, Department of Physics



Director, Honors Program

The Quantum Magneto Effect in Bismuth

Ömer Kerem Durdağ

St. John's University, Collegeville, MN 56321

May 22, 1991

Abstract

Using a standard field modulation technique, the de Haas-van Alphen effect was measured in bismuth for various crystal orientations. Measurements performed using a d.c. magnetic field that was ramped up from ~ 0.05 T to ~ 0.6 T at 4.2 K with a ~ 0.01 T modulating field. Data shows a variation of dHvA period with orientation that is in good agreement with the results of Bhargava¹.

Introduction

The de Haas-van Alphen Effect (dHvA) is a phenomenon of Fermi surface electrons. It was first discovered in 1930 by the two scientists, that the diamagnetic susceptibility (χ) of bismuth varies in an oscillatory manner as a function of a changing magnetic field. These oscillations were found to be periodic in inverse magnetic field ($\frac{1}{B}$) providing absolute knowledge of the

¹Bargava, R.N. "de Haas-van Alphen and Galvanomagnetic Effect in Bi and Bi-Pb Alloys," *Physical Review*. Volume 156, Number 3. April 15, 1967.

extremal cross-sectional area of the Fermi surface, and these results have been extensively published for various metallic and semiconductor crystals. The intent of this thesis was to duplicate a typical dHvA study of bismuth using the crystal orientation as a parameter. First, I attempted to understand the theory describing the effect and the formation of the Brillouin zones on the Fermi surface. Second, using available equipment and resources, I designed an experimental set-up that would allow for observation at various sample orientations via a field modulation technique, and finally, I actually observed the oscillatory phenomenon and collected data regarding the Fermi surface as a function of orientation. These three aspects of my research are discussed below.

Theory²

Since the de Haas-van Alphen Effect is a phenomenon of electrons, it is instructive to begin by considering a free electron gas—an acceptable model for conduction electrons in a metal. The electron will be in the lowest possible energy state specified by

$$E = \frac{(\hbar\vec{k})^2}{2m} \quad (1)$$

where m denotes the effective mass of the electron, and k is the momentum. By the Pauli Exclusion Principle each state is limited to two electrons of opposite spin, so at absolute zero, additional electrons must fill ascending energy states up to some maximum value. In k -space, or momentum space, these allowed energy levels would resemble a lattice (Fig. 1), where

²A major part of the below discussion is adapted from *The dHvA Effect in Bismuth* by Mary Amann.

each lattice point denotes a discrete energy value. The net result, however, is a quasi-continuum of energy values. The maximum energy level in this collection is the Fermi energy, denoted E_F . Electrons corresponding to this energy constitute the Fermi surface which is customarily the sharp boundary between occupied and unoccupied states in k -space. Hence, in this model the Fermi surface is spherical, but for most real metals this is not the case.

An energy distribution graph of these electrons (Fig. 2a) indicates that all states below the Fermi level are full, while all states above it are empty. Of course absolute zero can not be obtained in the laboratory. A finite temperature energy distribution (Fig. 2b) shows that some finite width of electrons below E_F are able to move to other states. These electrons are able to move because the thermal energy available to them, kT , is probabilistically sufficient to lift an electron from a filled state within the Fermi surface to an unfilled one outside it. Therefore only those electrons with energies within kT of the Fermi surface will contribute to the electronic properties, or more specifically, the magnetic susceptibility.

In order for any electron to contribute to the magnetic susceptibility however, it must be in a magnetic field. Classically, a free electron in a uniform magnetic field experiences a force

$$\vec{F} = \frac{q\hbar}{m} \vec{k} \times \vec{B} \quad (2)$$

If this magnetic field is directed parallel to k_z so that only the k_x and k_y components of the electron are affected with the Lorentz force acting on every electron, the electrons will follow a helix at the cyclotron frequency in real space, where the cyclotron frequency is denoted:

$$\omega_c = \frac{eB}{m} \quad (3)$$

The solution will now be derived quantum mechanically. Beginning with the Schrödinger equation for a free electron in a magnetic field

$$E\psi = \frac{1}{2m} \left(\frac{\hbar}{i} \vec{\nabla} - \frac{e}{c} \vec{A} \right)^2 \psi \quad (4)$$

(where the vector potential \vec{A} has been chosen so that \vec{B} is in the k_z -direction), it follows that the energy eigenvalues for the complete system are sums of eigenvalues for a two-dimensional harmonic oscillator in the k_x - k_y plane, and the eigenvalues for a free particle in the k_z direction, i.e.:

$$E = \frac{(\hbar k_z)^2}{2m} + (n + \frac{1}{2})\hbar\omega_c \quad (5)$$

where n is a quantum number taking on integral values. Hence, the resultant effect of the magnetic field is a re-quantization of the energy states. No longer do k_x, k_y, k_z describe the electron. Instead, a new quantum number n does. Ignoring the z coordinate in k -space, this new quantization scheme corresponds to circles of constant energy in the k_x - k_y plane (Fig. 3). The total number of electron states does not change with the introduction of the magnetic field however. The number of states with quantum number n on any given circle is exactly the number available amongst the allowed states in the annulus in which it lies when no B field is present. In three-dimensions, these circles are represented by a system of concentric cylinders, known as Landau tubes (Fig. 4). An increasing magnetic field causes the Landau cylinders to expand and eventually they must become empty as they pass out of the Fermi surface. Also the spacing between these tubes increases while the number of states remains constant as half the states move to higher energies, the other half moving to lower energies with the compensation being almost perfect.

When the radius of the Landau cylinder expands, the number of occupied

states that it contains decreases because its intersection with the spherical Fermi envelope shrinks. Eventually, when the radius becomes larger than k_F it empties completely. However, as a level empties, it causes the total energy first to decrease very slightly below the Fermi level, and then, when it passes through the former Fermi level, it causes the energy to increase somewhat. Thus every time a Landau cylinder passes through the spherical envelope a regular fluctuation in the total energy of the electron gas occurs.

There are now two conditions controlling which electrons can contribute to the magnetic susceptibility; their energy must be within kT of E_F , and they must lie on a Landau tube. It is at the intersection of these two constraints where the contributing electrons can be found. It is obvious that these intersections are rings with thickness kT and the same cross-sectional areas as the Landau tubes where the area between two adjacent rings is:

$$\frac{2\pi eB}{\hbar} \quad (6)$$

For the inner tubes, very few states contribute. But if the Landau tube is tangent to the Fermi surface, a finite width contributes. Such a tube necessarily represents an extremal cross-sectional area (A) of the Fermi surface:

$$\frac{\partial A}{\partial k_z} = 0 \quad (7)$$

where $A = \pi(k_x^2 + k_y^2)$. Recalling that the two-dimensional oscillator term in the energy eigenvalue solution (Eq. 5) can be written as $\hbar^2(k_x^2 + k_y^2)/2m$, this area is expressed

$$A = (n + \frac{1}{2}) \frac{2\pi eB}{\hbar} \quad (8)$$

As the magnetic field is varied, the number of states contributing will fluctuate between very small and very large values as successive Landau tubes

become tangent to the Fermi surface. Solving Eq. 5 and Eq. 8 for successive maxima of the oscillations results in sinusoidal oscillations dependent on the inverse magnetic field, hence the oscillatory phenomenon of the magnetic susceptibility observed by de Haas and van Alphen

$$\chi \sim \sin \left(\frac{\hbar A_{\text{ext}}}{2e} \cdot \frac{1}{B} \right) \quad (9)$$

where A_{ext} is the extremal cross-sectional area of the Fermi surface. Thus far I have presented a very general theoretical explanation of the cause of the de Haas-van Alphen effect. A more rigorous approach will also yield the expected magnitude of the effect. Quoting these results³,

$$\chi \propto e^{c_1\tau/B} e^{-c_2T/B} \sin \left(\frac{c_3}{B} A_{\text{ext}} \right) \quad (10)$$

From these two equations, many important experimental criteria can be extracted. The factor of τ (mean collision time) in the first exponent indicates that a long mean free path is necessary. Thus, the electrons must be free to orbit without scattering, so this necessitates an extremely pure single crystalline sample. The factors of B in the second exponent and the sine term point to the need of a large uniform magnetic field (~ 0.6 T). The factor of T shows the need for low temperature (~ 4 K). This condition follows because the Landau levels are considerably broadened at higher temperatures, so only low temperatures produce sharp oscillations.

At this point a detailed discussion of the Fermi surface of bismuth is essential. The Fermi surface of bismuth consists of three electron ellipsoids and one hole ellipsoid (Fig. 5). The hole ellipsoid is a spheroid of revolution

³Stark, R.W. and L.R. Windmiller. "Theory and Technology for Measuring the de Haas-van Alphen Type Spectra in Metal," *Cryogenics*. October 1968.

about the k_z axis. With respect to the crystal axes k_x the binary, k_y the bisectrix and k_z the trigonal axis the equations for these ellipsoids are, for the electrons:

$$a_1 k_x^2 + a_2 k_y^2 + a_3 k_z^2 + 2a_4 k_y k_z = 1 \quad (11)$$

together with two others obtained by rotation through $\pm 120^\circ$ about the k_z axis (in order to satisfy the rhombohedral symmetry), and for the holes:

$$(k_x^2 k_y^2)/h_1^2 + k_z^2/h_3^2 = 1 \quad (12)$$

The best fit to Edelman's⁴ data gives:

$$a_1 = 3.494 \times 10^{-12} \text{ cm}^2, \quad (13)$$

$$a_2 = 0.0404 \times 10^{-12} \text{ cm}^2,$$

$$a_3 = 1.987 \times 10^{-12} \text{ cm}^2,$$

$$a_4 = -0.2206 \times 10^{-12} \text{ cm}^2$$

The significance of the cross-term $2a_4 k_y k_z$ is that the principal axes of the ellipsoid are tilted in the k_y, k_z plane from the k_y and k_z axes, the numerical data correspond to a tilt angle of $\theta = 6.38^\circ$. The principal axes lengths given by:

$$e_1 = a_1^{1/2} = 0.535 \times 10^6 \text{ cm}^{-1}, \quad (14)$$

⁴Edelman. V.S. (1976) *Advances in Physics*. **25**, 555. The fit is in fact good to only a few %, but the a_i are given to four significant figures so that they should be consistent with the lengths of the principal axes as given by the e_i . In particular the value of e_2 in terms of the a_i depends on the difference of two nearly equal quantities and is therefore extremely sensitive to the values of the a_i .

$$e_2 = 7.98 \times 10^6 \text{ cm}^{-1},$$

$$e_3 = 0.705 \times 10^6 \text{ cm}^{-1}$$

The hole ellipsoid is one of revolution about the k_z axis and its principal axes are:

$$h_1 = 1.391 \times 10^6 \text{ cm}^{-1}, \quad h_3 = 4.628 \times 10^6 \text{ cm}^{-1}. \quad (15)$$

It can easily be seen that the dimensions of the both the electron and hole ellipsoids are indeed small compared to the Brillouin zone dimensions which are of the order 10^8 cm^{-1} and calculation shows⁵ that the volume v of the three electron ellipsoids is $37.8 \times 10^{18} \text{ cm}^{-3}$, which is within experimental error equal to that of the hole ellipsoid, $37.5 \times 10^{18} \text{ cm}^{-3}$ as would be expected for a compensated semi-metal where $n_e = n_h$.

Experimental Method

Instrumentation

Observation of the de Haas-van Alphen effect was achieved by employing a standard field modulation technique. The single crystal bismuth sample was attached on a sample holder⁶ within a crystal chamber on our designed probe that also had a counter-wound pick-up coil⁷. The entire rotation unit was cooled to liquid helium temperatures, and exposed to a sweeping magnetic

⁵Schoenberg.D. *Magnetic Oscillations in Metals*. Cambridge: Cambridge University Press. 1984. Page:229-230.

⁶For our first experiment run we used Apiezon grease grade "N." For our second run we used nail polish which worked better.

⁷Please refer to the discussion on the section "Probe" for a detailed treatment.

field of ~ 0.05 T– ~ 0.6 T. A variable a.c. modulating field (~ 5 – 100 Gauss), which was in turn provided by a 140 Hz sinusoidal signal from the Wavetek Model 23 function generator and amplified by one channel of the 60 W Kenwood amplifier, produced a voltage in the pick-up coil. A 5Ω series power resistor was used between the power amplifier and the modulating coil to present a proper load impedance to the amplifier. The signal was roughly proportional to the magnetic susceptibility χ' for $2f$ measurements. The signal was then detected on an EG&G Model 5209 lock-in amplifier on which a band pass filter and “track” mode were utilized. The time constant, phase and sensitivity of the lock-in were varied for maximum signal detection. The signal was generally measured at $2f$ to avoid the large pick-up effect present at the fundamental frequency⁸. Before reaching the differential inputs of lock-in, the signal voltage was increased by a factor of ~ 15 in an impedance matching transformer, and filtered by a high-pass filter to attenuate the $1f$ signal. These connections were all made via polypropylene-shielded, miniature audio cables (Belden 9452), and miniature audio connectors (Switchcraft tiny “Q-G”) obtained from Newark. Banana jacks from the analog output of the lock-in and the d.c. power supply (via a current buckler⁹) led to the chart recorder which produced the plots (which showed clearly the dHvA effect), where the y -axis measured the strength of magnetization of the Bi sample and the x -axis recorded the field current in amps (Fig. 6).

⁸At $1f$, signals were observed, though they contained noise and were excluded from our final data analysis.

⁹The current buckler was manufactured at St. John’s and mainly assists in eliminating excess d.c. offsets from the system.

Sample Preparation¹⁰

Preparation of the required bismuth single crystal was a major undertaking in the experimental preparation. Because of prohibitive cost, it was not feasible to purchase a pure crystalline sample. This meant that the crystal had to be grown. A 99.9999% pure poly-crystalline bismuth rod was ordered from AESAR for sample preparation.

The crystal was grown by the Czochralski technique. A seed crystal was first prepared from the 99.9999% pure bismuth rod. Approximately 15 grams of the rod were placed in the small (~ 3 mm) diameter glass tube, one end of which had been sealed using a propane torch. The tube was then connected to the forepump and cold trap to catch any pump oil vapor that may have escaped from the pump. The tube was heated under vacuum using the propane torch until all the Bi rod was completely melted. The surface of the liquid Bi was then slowly heated while the lower end was allowed to cool. Upon cooling to room temperature, the sample was removed from the tube by carefully shattering the glass. The seed was then cleaned with 6M HNO₃ for three minutes to remove any impurities that may have come from the tube.

The seed crystal was attached to the crystal growing rod using nickel-chrome wire. The crystal chamber was heated to 275°C. During heating, the aluminum oxide crucible containing approximately 85 grams of 99.9999% pure Bi rod which had been cleaned for three minutes in 6M HNO₃ was rotated at 3 RPM to insure even heating. When all the rod in the crucible

¹⁰For a detailed treatment of bismuth sample preparation, refer to *The dHvA Effect in Bismuth* by John Weidner.

had liquified, the seed crystal was plunged approximately 3 mm into the melt in the crucible. The crucible rotation was then stopped to keep any floating sludge on the surface of the Bi from interfering with crystal growth. The seed was rotated at 6 RPM and was pulled up at a rate of 3 inches per hour.

After about two hours, a large crystal had grown onto the seed. The seed near the beginning of the crystal and the bottom $\frac{3}{4}$ " of the crystal were cut using a hacksaw. Approximately 1–2 mm of each end of the crystal was removed using 12M HNO₃ in order to eliminate any part of the crystal that may have been impure or damaged from sawing. Finally the entire sample was submerged in 12M HNO₃ for 3 minutes to clean the entire surface and to see the underlying structure more clearly.

Cryostat

The low temperature conditions necessary for the experiment were achieved with a Cryofab nitrogen-jacketed liquid helium dewar. Although liquid helium is a somewhat costly cryogen (~\$6/L), its STP boiling point temperature of 4.2 K (and ability to be further reduced to 2.2 K by implementation of the λ -plate), provided the low temperature environment essential for observation of the de Haas-van Alphen effect.

Surrounded by a vacuum space and a liquid nitrogen jacket, the liquid helium was contained within the stainless steel dewar (Fig. 7a). The vacuum and nitrogen shielding, together with the copper radiation baffles on the magnet supports and the probe itself, helped in reducing the introduction of detrimental amounts of heat into the system given the low boiling point of helium (Fig. 7b). Two days before the experiment, the vacuum chamber of

the cryostat and the stainless steel helium transfer tube were pumped out to $\sim 10^{-6}$ torr with a diffusion pump. On the experiment day, the jacket was first filled with approximately 20 L of liquid nitrogen. The inner chamber was then precooled with liquid nitrogen enabling us to use a minimum of helium. When the volume of LN_2 in the reservoir was a maximum, the carbon resistor read $\sim 72 \Omega$, which later provided us with a rough gauge for the temperature fall in the system during the experiment. The liquid was then removed and recycled via the same path by pressurizing the reservoir with gaseous helium through the vapor-cooled current leads.

Transfer of the liquid helium into the reservoir was then executed. A vacuum insulated transfer tube (made of stainless steel) was fitted with extensions reaching from the bottom of the helium storage dewar (borrowed from the University of Minnesota) to the bottom of our cryostat. The liquid helium was then pumped through with pressure from a tank of gaseous helium. The level was slowly and gradually allowed to achieve a maximum of 51 cm. Thus approximately 11 L of helium had collected, although nearly 15 L from the original 33 L supply were consumed. At 4.2 K, the carbon resistor read 840Ω . Having a boil-off rate of approximately 1.5 L/hr, the life of this quantity of helium was a little over seven hours; after that time the magnet was no longer covered and data taking was not deemed possible because of the danger of quenching the magnet.

On the second run day, the LN_2 jacket was refilled for the purposes of the precooling procedure. The helium reservoir was filled to the 62 cm height, consuming the balance of the original 33 L supply. The λ -plate was then utilized by reducing the gaseous helium pressure in the tube above the plate

with a Cenco mechanical pump. The pump was isolated from the rest of the system with the use of vibration reduction pads. The plate was found to operate most efficiently when the needle-valve was $\frac{3}{4}$ turns open¹¹.

While the pump was running, the reading on the carbon resistor dramatically increased, eventually peaking at 2420 Ω , a value over three times that at 4.2 K. Although there was no means of confirming an actual temperature, it is suspected that at this resistance the temperature was reduced to perhaps very near to 2.2 K. At this low temperature, it was also observed that the system was extremely sensitive to heat inputs but produced excellent data. To reduce the effects of heat input, the multimeters, persistence switch and amplifier were shut off, except when data was being taken. Use of the λ -plate affected the LHe boil-off rates. During its operation, rates were calculated to be almost 2.5 L per hour, consequently allowing for over 7 hours of uninterrupted de Haas-van Alphen observations.

Magnet

A custom designed superconducting solenoid magnet from Cryomagnetics, Inc. provided the necessary large magnetic fields. When immersed in the liquid helium of its companion cryostat, two separate coil windings of 1641.9 (inner) and 9126.3 (outer) turns each (Fig. 8) make possible the maximum 10 T field. The main d.c. coil is also lined with three individual counter-wound coils which allows for an a.c. modulation. In addition, the system is equipped with a persistence switch, providing the ability to maintain a constant magnetic field with no need for a power supply. When operating in

¹¹The mercury barometer that was connected to the pump and the valve read 60cmHg.

non-persistent mode, the power source is a 100 A power supply, also manufactured by Cryomagnetics, capable of current and magnet voltage monitoring as well as gradual ramping.

Probe

The probe consists of the gearbox/sample holder that allows us to rotate the sample, the coil that gives us a pick-up signal, a connecting ring and a brass top which allows us to hook up the probe apparatus to the electronics.

The probe was painstakingly constructed after many technical difficulties in the SJU Machine Shop. The gearbox and the coil form are made out of phenolic, except for the spur and worm gears, which are made out of Delrin (Fig. 9,10,11,12,13).

The highlight of the design of the gearbox is the mechanism which enabled us to rotate the crystal within the crystal chamber. Restricted by a maximum diameter of one inch (the inner diameter of the modulating field coil), material elasticity and acutely precise measurements, the rotation of the sample was an exercise in engineering and design; the results show a simple and effective functioning. By a transfer of circular motion by the spur-worm gear combination, one full rotation of the crystal is made possible by eighteen turns of the worm gear.

The worm was pressure fitted (within the gearbox) to a $\frac{1}{16}$ " phenolic rod. The spur gear (brought from Boston Gear; the hub was later shaved off) is held in place (pressure fit) by the shaft of the sample holder which bores through the adjacent wall of the crystal chamber through the slot in which the spur gear is placed (Fig. 9). The spur gear rotates by meshing

with the custom-made worm gear (constructed with 16 teeth/inch), and in its rotation drives the shaft of the sample holder, thereby rotating the bismuth crystal. The thermal expansion coefficient of the materials were such that (the thermal coefficient for Delrin is greater than that for phenolic), the pressure fitting became even stronger when the temperature was lowered as indicated by the table below:

Material	Coefficient of Thermal Expansion ($\times 10^{-6}C^{-1}$)
Delrin	90
Phenolic	81
Steel	15 - 17
Brass	20

Table 1.

The $\frac{1}{16}$ " phenolic rod is connected to a $\frac{1}{16}$ " stainless steel tube with a connector junction constructed from aluminum. The $\frac{1}{16}$ " stainless steel tube runs to the top of the brass plate enclosure at the top of the cryostat, from where it can be manipulated for rotation. The 36 gauge wires to the coil from the connector on the brass plate (where all the electronic connections are situated) at the top travel down the $\frac{1}{4}$ " diameter steel steel tubing that is screwed (0-80 screw) to the $\frac{1}{4}$ " shaft in the center of the gearbox. The wires then go through a hole on the side of the gearbox to find their destination on the solder terminals. At the base of the gearbox, a circular groove was cut, 0.039" deep and 0.650" in diameter, on which the coil form was attached with a collar. The collar was slid over the top part of the coil form and screwed on to it and then with countersunk holes screwed to the gearbox (Fig. 13).

The coil form, consists of two spindles to accommodate coils of opposite flux. All the dimensions of the coil (radius, length) affect the signal that it can produce. In order to help the coil design process a computer program written by Dr. Kirkman was used¹². The program calculated the essential individual and total flux densities of the coils together with the $d\Phi/dz$ ratios and dipole strength. Our aim was to get the two coil voltages to cancel each other out in the absence of a sample, while keeping $d\Phi/dz$ small and at the same time have an appreciable dipole strength. One of our important considerations was the physical strength of the phenolic regarding its ability to stand pressure for machining. Nevertheless, after numerous theoretical calculations and experimental tryouts, the final coil form design was achieved (Fig. 10).

It is important to add here that the philosophy in designing the coil form was to have the coils as close to the sample as possible within the limitations of the machinability of the phenol. Also at the same time we wanted to get as many turns of coil as possible for the greatest dipole strength but only if it resulted in the cancellation of the top and bottom coil voltages. Needless to say, it was a balancing act, with compromises in size and total voltage cancellation and dipole strength, in end resulting in the final design.

The coils were wound on the lathe with opposite direction with respect to each other, using a 40 gauge wire. The top coil has 3123 turns (with a resistance of 417 Ω at room temperature) while the bottom coil has 3390 turns (with a resistance of 474 Ω at room temperature). On the coil form itself, two terminals were constructed using a 24 gauge wire as terminal ends

¹²Program name is "Real_coil_flux" and is located in the [faculty.faculty.tkirkman.dhva] directory.

and attaching it in a hole in the coil form with glue (Silicon Rubber). It is on these terminals that the wires from the connectors on the top brass plate were soldered to the ends of the coil to form our pick-up coil circuit.

On the coil form, three 0.05" deep recesses were milled out, on which three Cu-Be strips were screwed down (0-80 size), in order to minimize the vibration of the phenolic probe within the modulating field. The strips were simply bent into their shape as slightly parabolic "springs" and touched the bore wall of the magnet. There is also a groove that runs the length of the coil form which allows the wires to reach their destination without being exposed on the surface.

Finally, the coil voltages were carefully balanced (to have the voltages of the coils cancel each other out in the absence of a sample) to an accuracy of $\frac{1}{10}\%$. The modulating field was activated at room temperature by a function generator at a frequency of 140 Hz and the lock-in amplifier was used to accurately detect the degree of voltage cancellation.

During the final experimentation itself, the center of the crystal sample was placed 0.27" (~ 1 mm) below the center of the modulating coil. This was done to compensate for the differential contraction of the $\frac{1}{4}$ " steel tubing relative to the epoxy/fiberglass magnet supports at 4.2 K, which we approximated to being 1 mm¹³.

The gearbox and coil form attachment was connected to the stainless steel tube that was soldered to its brass cap. This was seated over an o-ring on the lid of the dewar and held in place with six 6-32 screws. The brass top contained the electric connections from wherein the pick-up signal could

¹³Richardson, Robert C. and Eric N. Smith. *Experimental Techniques in Condensed Matter Physics at Low Temperatures*. New York: Addison-Wesley, 1988. Page 121.

be directed to the circuit that enabled us to take our data. The brass top was constructed by having two concentric brass cylinders (Fig. 12). Both cylinders rested on a brass plate on which they were soldered. Another brass plate, with a slot on its side was screwed on to the larger brass cylinder with 0-80 screws. The brass cylinder with the smaller diameter functioned like a chimney through which control rod passed, enabling the rotation of the sample.

Three connectors are imbedded in the separate lid: a banana plug to be connected to ground, a "Q-G" miniature socket for monitoring the carbon resistor, and a second "Q-G" for the pick-up coil signal. Removal of the lid reveals the 36 gauge twisted copper wire pairs leading to the "Q-G"'s as well as a spare wire pair. The wires are sealed to the $\frac{1}{4}$ " stainless steel tube with Silicon Rubber cement. The ground on each of these connectors was soldered to the ground banana plug.

There is a brass knob that is attached to the control rod on which a pointer and a circular scale with soldered. The control rod entry points on the "chimney" are vacuum sealed.

On the $\frac{1}{4}$ " stainless steel tube, four copper disks were punched and soldered to fit snugly inside the copper baffles on the magnet support, acting as heat shield. They were off-set $\frac{1}{4}$ " above the outer baffles, thereby minimizing radiant heat without impeding helium gas flow up the reservoir.

Results

Typical sweeps were made from 0.05 T to 0.6 T, where the current sweep rate was 0.011 A/s and the current to B field ratio was 822.5 G/A. A sample data

for the sweep at 120° is shown in Fig. 14. Successive sweeps were taken as the orientation was varied in 10° increments and plots of a lock-in signal versus the changing magnet current were simultaneously produced. The resulting data is summarized in Table 2. The lock-in phase was 172° , the frequency was 128 Hz and the modulating current was 334 mA (rms). The data for each sweep was digitized producing " χ " vs. $\frac{1}{B}$ plots from which de Haas-van Alphen periods for the oscillations were calculated (an example plot is shown in Fig. 15). Unlike the magnitude of χ , the dHvA frequency was found to be independent of modulation current or temperature but dependent upon orientation¹⁴. We initially found that the 30 chart recordings (Table 2) yielded confusing information. Converting the digitized dHvA charts to plots of period of oscillation as a function of angle gave a scatter plot, shown in Fig. 16. The data points in Fig. 16 are a result of using the SIDPLOT program to analyze the data, without the calibration of the zero point of the chart plots. Going back to our original charts, our zero points were recalibrated and axes scales were corrected. Upon replotting the correction, the results were still not encouraging¹⁵.

Approaching the interpretation of the data from another perspective, we fitted the values of periods from the digitized plots (using the FIT program) and observed the displacement factor (ΔB) that was necessary for our data to have the correct calibrated zero point (Fig. 17 shows the plot of our data

¹⁴Current was also set at 164 mA for some data readings but did not register a significant difference. However the data at low temperatures yielded plots that exhibited the dHvA effect most clearly without much noise or distortion.

¹⁵One chart plot that was made with varying angles but *constant* magnetic field showed a peak only from angles that ranged from 110° – 180° indicating our data was unintentionally selective.

analyzed with FIT, together with the ΔB factor taken into consideration). As Table 2 demonstrates, there are some angles which require a great readjustment. Also there are angles which give diverse period readings (for fitted and unfitted calculations). At the same time we were at a disadvantage because we were unable to obtain a dHvA signal at angles from 30° – 90° (signals at these angles merely was the noise from the pump or noise of the system).

As a final bid to check the validity of our data we checked the original charts if beats were recorded (a normal phenomena in dHvA effect observation; see Fig. 18 for a digitized plot). Those angles with an evident beat were ignored if they had given diverse period calculations. The angles which we finally admitted to be representative of the function of the period as a function of angle were those which had a low displacement factor value (ΔB), had little variance of period calculation over two or more attempts and which were within the close region of the values of periods for respective angles that was measured by Bhargava.

Table 2 upon further observation yields valuable insight to our data. The table shows that many of the points for reasons due to mistaken calibration or simply bad luck demonstrate that their zero points are not where we thought they were. The displacement factor is simply an added factor to the $\frac{1}{B}$ in our function that we initially used to calculate the frequencies of the oscillations. The unfitted data for the majority of the angles differs greatly from the fitted version which is of concern when trying to ascertain the relationship between period and rotation angle. The temperature difference does not explain the discrepancy, neither do the time constant changes. Upon analysis of beats, there was no consistency between the data points, leading one to surmise that

the data was not good to begin with due to a weak signal¹⁶. The purpose of having the fitted (using FIT program) and unfitted (obtained simply from the SIDPLOT program) data is to show the variance of our data points that we finally did use from using different fitting programs. The SIDPLOT data points assumes that the calibration of the chart recorder (our zero points and scale) was correct while the FIT program was used to see if indeed that was true. The final validity of the points that were used for our final plot consists in having low displacement factors and the fact that the points clearly form a curve similar to the one obtained by Bhargava.

Our error analysis consisted in taking the errors measured for the frequencies by the SIDPLOT and FIT programs for our respective angles and simply converting them, using error analysis derivative equations (using the basic relationship between period, frequency and the conversion factor of amps to gauss). Obviously the only error we are taking into consideration is the error in our digitization process. Other errors arising from the construction of the equipment and the system itself were neglected because we ourselves were not sure of it.

The final plot of our data is quite similar to that obtained by Bhargava¹⁷ (Fig. 19). Even though we do not have the characteristic dip of the curve at 60° it is evident that our data yields a curve similar to Bhargava. Whether it is the SIDPLOT or FIT curve, there is close agreement with Bhargava's data and in fact more than one point overlaps with each other. The curvature of all three curves is evident, though it may be hard to see it in our curve due

¹⁶This was not observed on the scope that was connected to the lock-in amplifier output.

¹⁷Bargava, R.N. "de Haas-van Alphen and Galvanomagnetic Effect in Bi and Bi-Pb Alloys," *Physical Review*. Volume 156, Number 3. April 15, 1967.

to the lack of data at many angles. By filling in the gaps present, our data appears valid. This data demonstrates that the bismuth crystal was rotated in the binary-trigonal (xz) plane. The two curves that were obtained by Bhargava indicating dual period calculations for a single angle are roughly evident from our plot too.

Conclusion

A field modulation technique was employed to observe the de Haas-van Alphen oscillations in bismuth for various crystallographic orientations. It is clear from our data that the crystal was rotated in the binary-trigonal plane and that in agreement with Bhargava's data, we not only observed the dHvA effect but a relationship between the period of oscillation and of rotation angle. Our data though not ground breaking, was a testament to designing an undergraduate research project that was joyfully parallel in demonstrated results to that of established physicists.

Our results would have been more extensive and accurate if we were not limited by the amount of helium. Since the second run was practically a repetition of the first instead of being a further indepth investigation (changing modulation frequencies, phase and time constants) with an established preliminary data analysis, we were not able to overcome our mistakes (not marking our zero points very carefully, smaller angle increments) and shortcomings (pump and system noise). But nevertheless the enormous success of our project lies in the apparatus that was designed and implemented, yielding a wealth (albeit sometimes confusing!) of information on the dHvA effect.

The scope of dHvA research lies only in the imagination of the experi-

menter. With the rotation unit functional, dHvA effects in impure samples or alloys could be observed. Fermi surfaces of various other metals could be mapped and a variety of complicated oscillatory and magnetoacoustic phenomenon could also be investigated.

Acknowledgements

I am enormously indebted to my advisors and mentors at St. John's University: Dr. Chuck Lavine and Dr. Tom Kirkman. There is no doubt in my mind that without their sense of humor, patience, confidence in me, and experience, this thesis would be still in the stages of wishful thinking.

I also want to thank my friend and helper at every available hour, Adam Whitten; his invisible presence made this project possible. And without my partner, John Weidner, I would not have had a crystal. Somehow, both of us, made this experiment worthwhile and fun.

I am grateful to the entire Physics and Honors Department for their assistance in the completion of this project, specially to my thesis readers, Dr. Dean Langley and Dr. Carol Theisen, whose encouragement has proven to be invaluable to me.

I would like to dedicate this 12 month project, over which I transcended sleep, visions of futility and insanity, to my late father, Ismet Durdağ.

References

1. Amann, Mary. "The de Haas-van Alphen Effect in Bismuth," *Senior Thesis, Physics Department, Saint John's University*. June, 1989.
2. Bargava, R.N. "de Haas-van Alphen and Galvanomagnetic Effect in Bi and Bi-Pb Alloys," *Physical Review*. Volume 156, Number 3. April 15, 1967.
3. Coffey, Mike. Cryofab, Inc. (615) 482-9551.
4. Hurd, C.M. *Electrons in Metals*. New York: John Wiley & Sons, 1975.
5. McClintock, P.V.E., D.J. Meredith and J.K. Wigmore. *Matter at Low Temperatures*. London: Blackie, 1984.
6. Myers, H.P. *Introductory Solid State Physics*. London: Taylor & Francis, 1990.
7. Richardson, Robert C. and Eric N. Smith. *Experimental Techniques in Condensed Matter Physics at Low Temperatures*. New York: Addison-Wesley, 1988.
8. Stark, R.W. and L.R. Windmiller. "Theory and Technology for Measuring the de Haas-van Alphen Type Spectra in Metal," *Cryogenics*. October 1968.
9. Weidner, John. "The de Haas-van Alphen Effect in Bismuth," *Senior Thesis, Physics Department, Saint John's University*. May, 1991.
10. Ziman, J.M. *Principles of the Theory of Solids*. Cambridge: Cambridge University Press, 1964.

k - Space

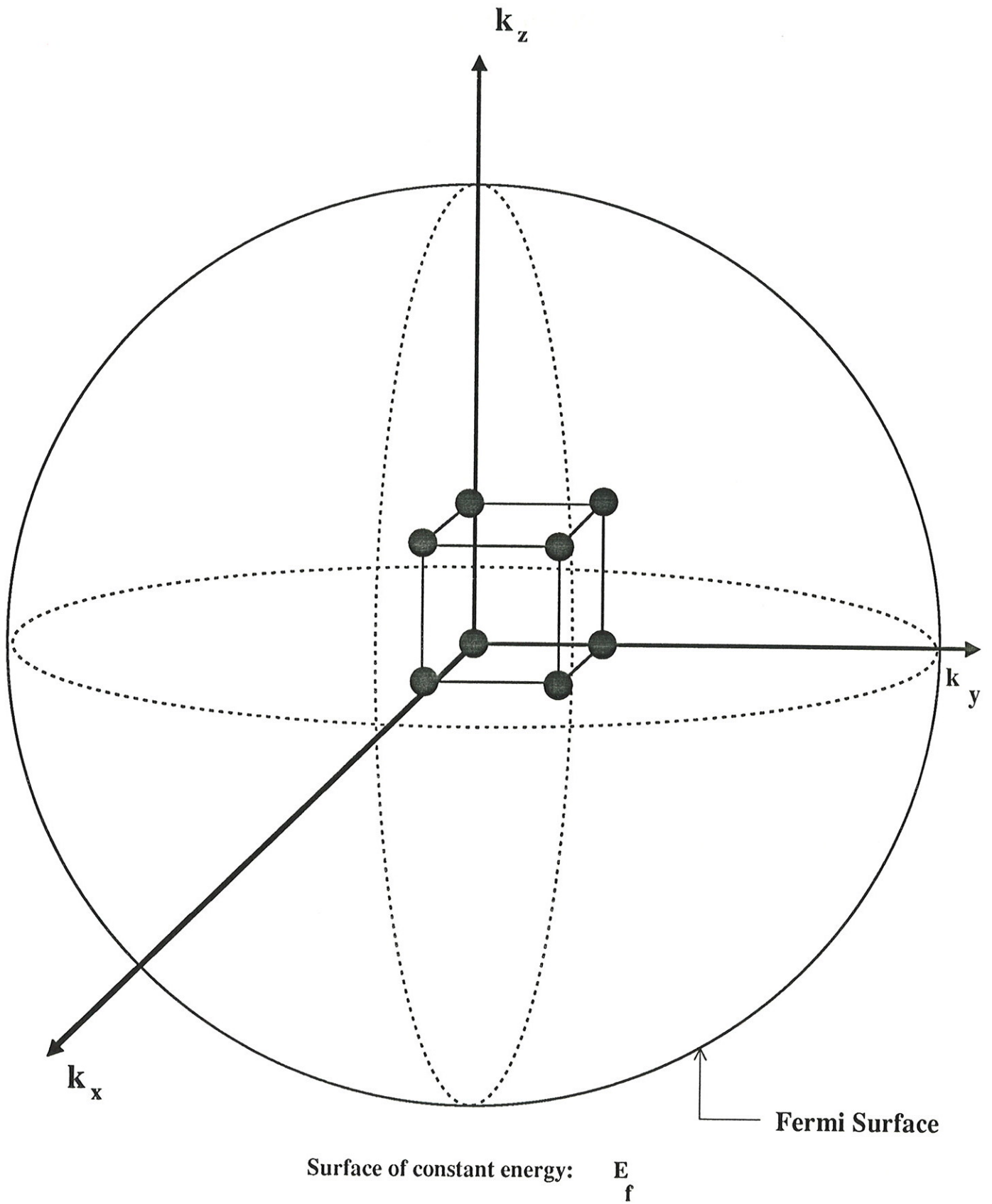


Figure 1

Energy Distribution

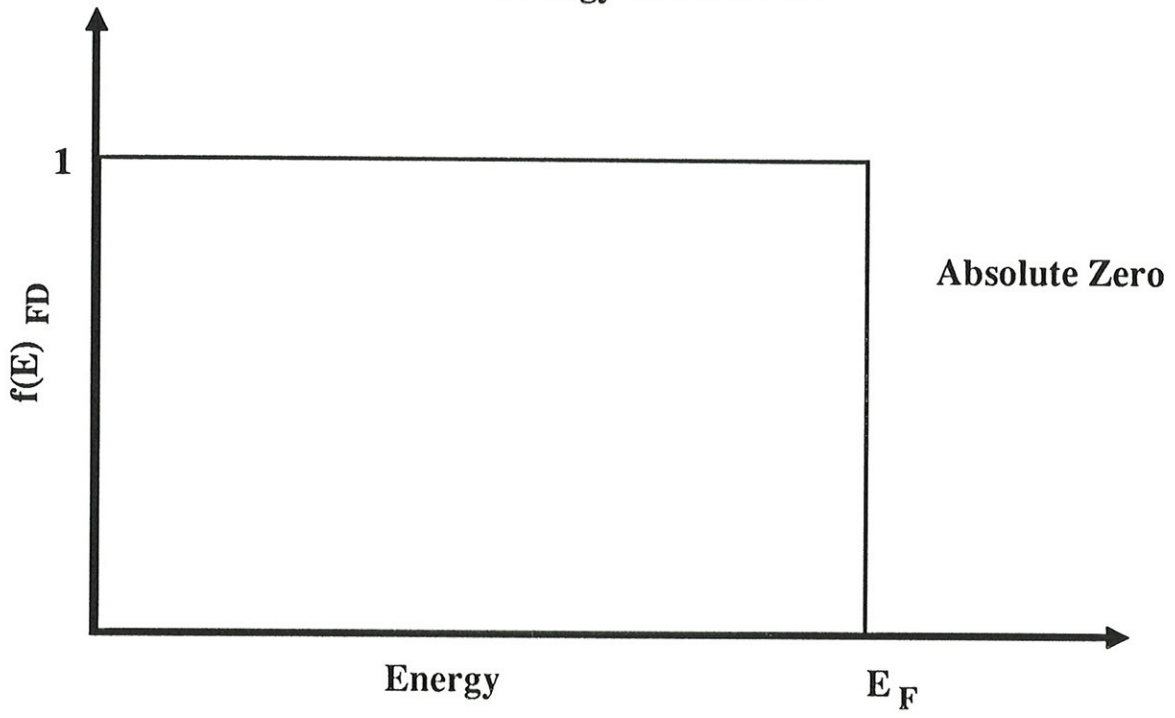


Figure 2a

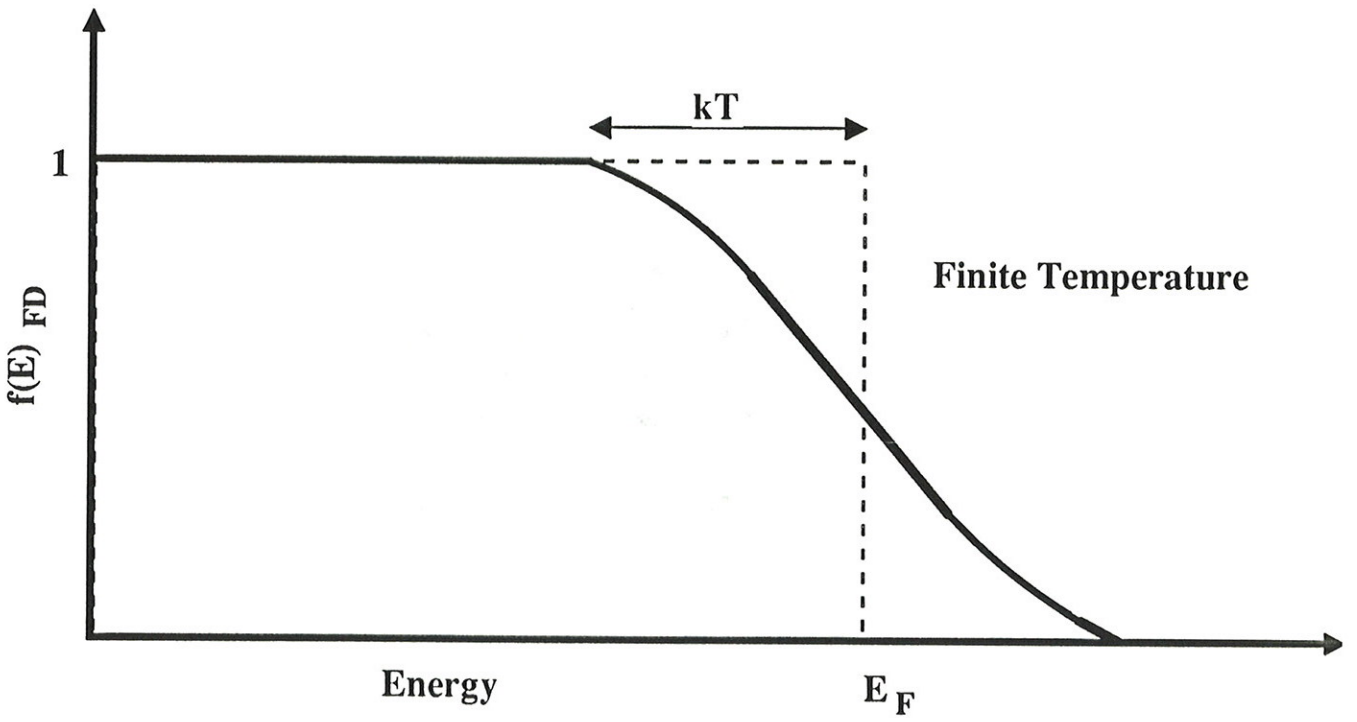
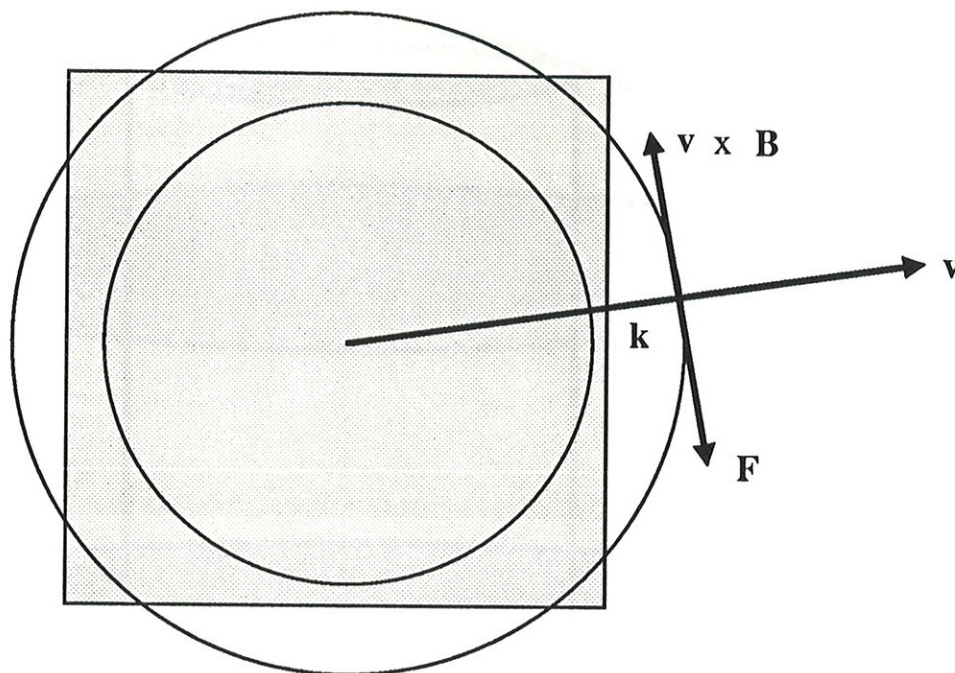
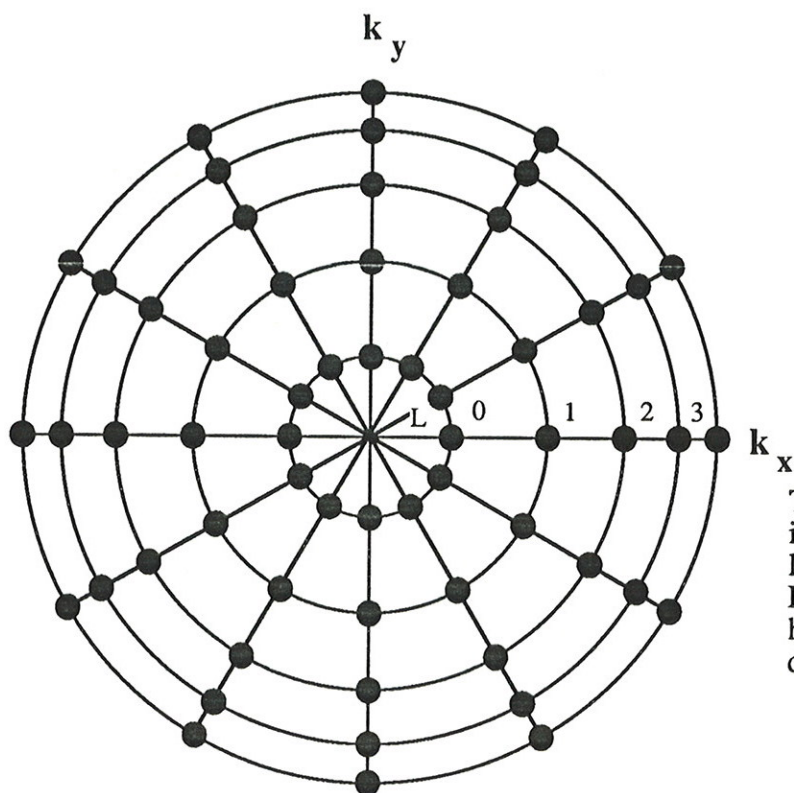


Figure 2b

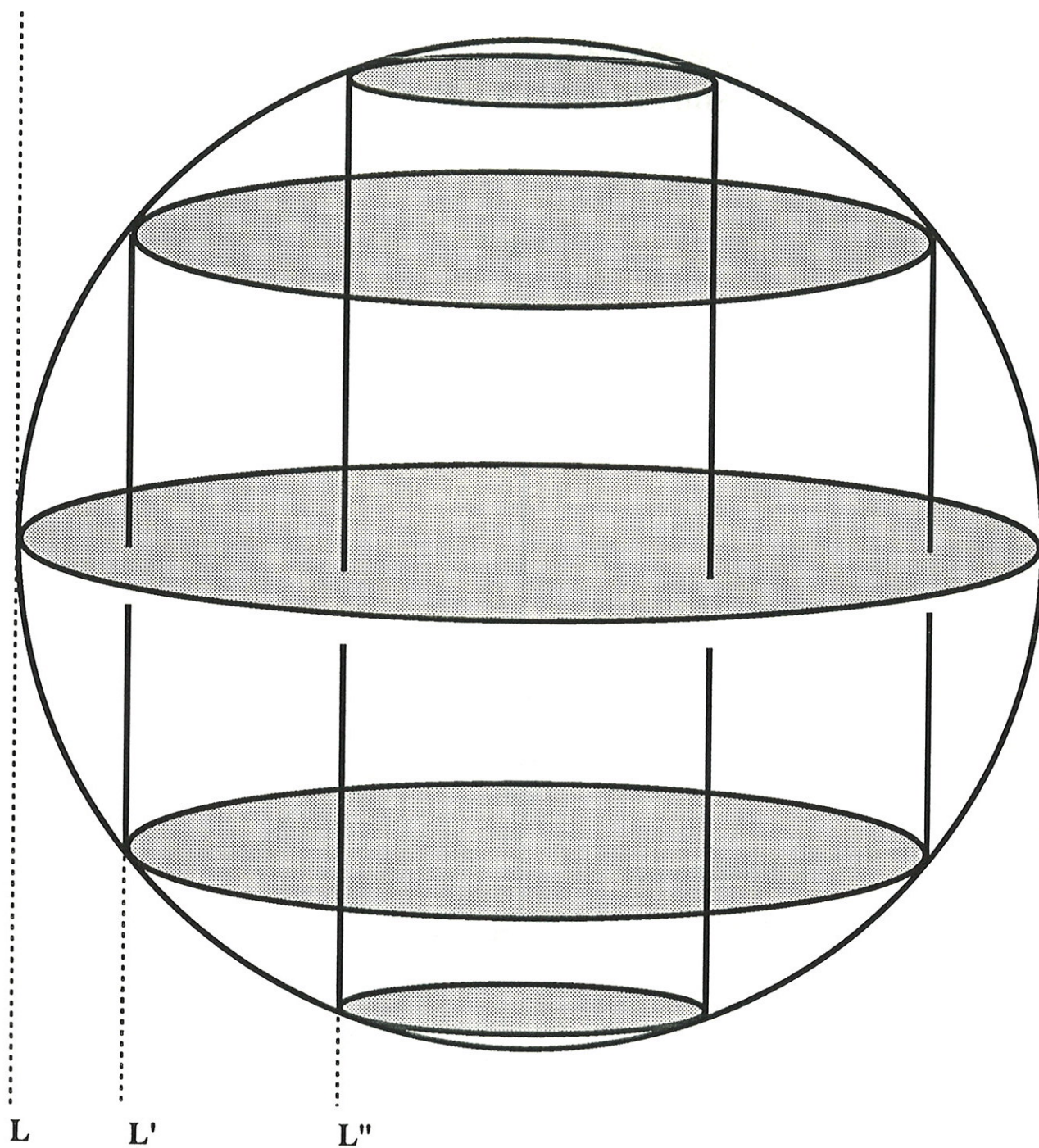


A plane section through k -space. The allowed electron states arise as an infinite uniform distribution of representative points. In the presence of a magnetic field B directed normally into the plane section, each k state is subject to a Lorentz force and all the k states rotate with the cyclotron frequency about an axis through the origin and parallel to the field direction.



The cyclotron motion introduces quantized levels, the Landau Levels. Each level has the same degeneracy.

Figure 3



The free electron gas has a spherical Fermi surface, but in the presence of a strong magnetic field we find the system of concentric cylindrical Landau levels. The occupied portions of these levels are determined by the original Fermi sphere. An increasing magnetic field causes the Landau levels to expand, and eventually they must become empty as they pass out of the Fermi sphere.

Figure 4

Location of Fermi Surface of Bismuth in the Brillouin zone

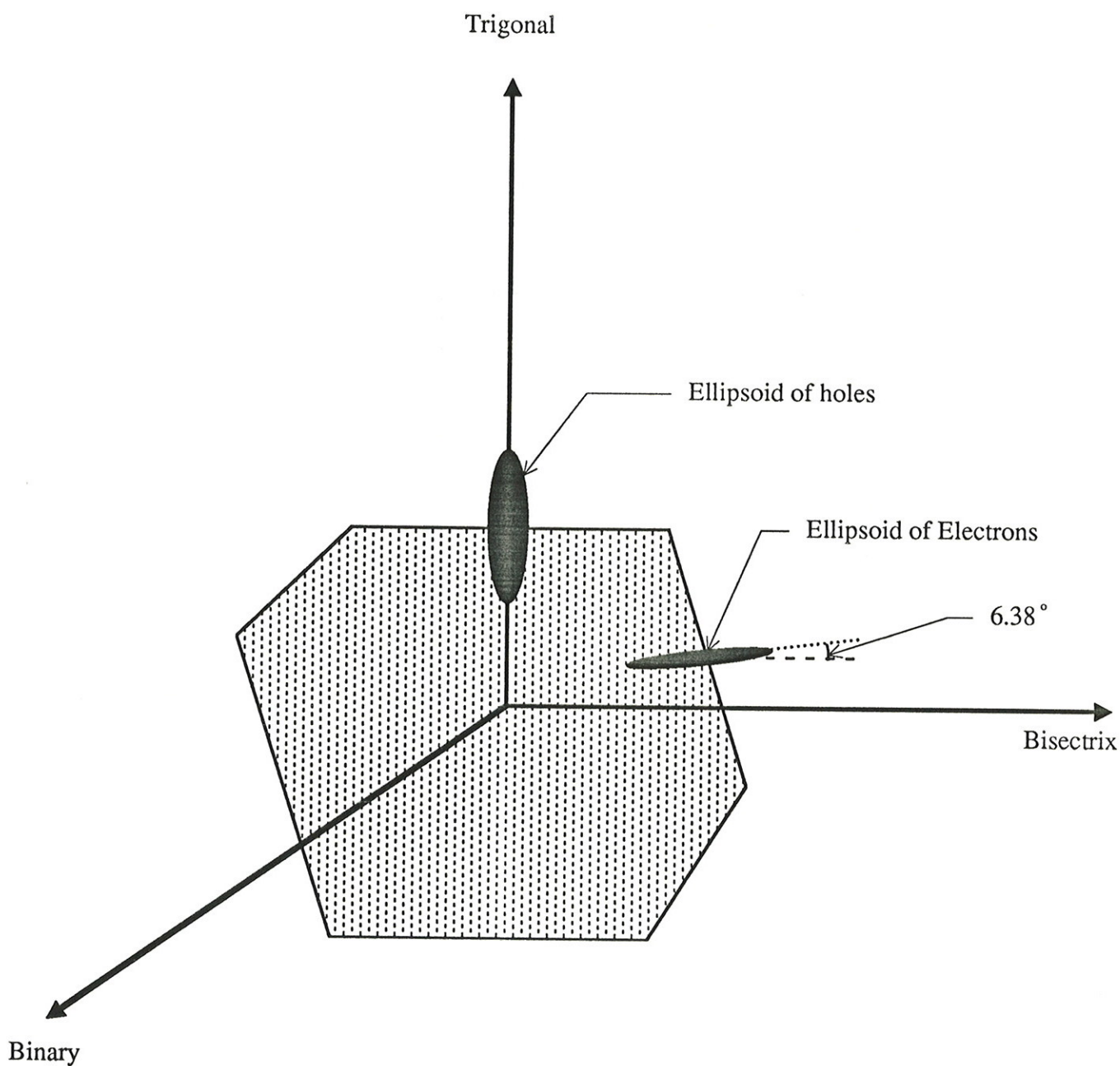


Figure 5

Experimental Set-Up

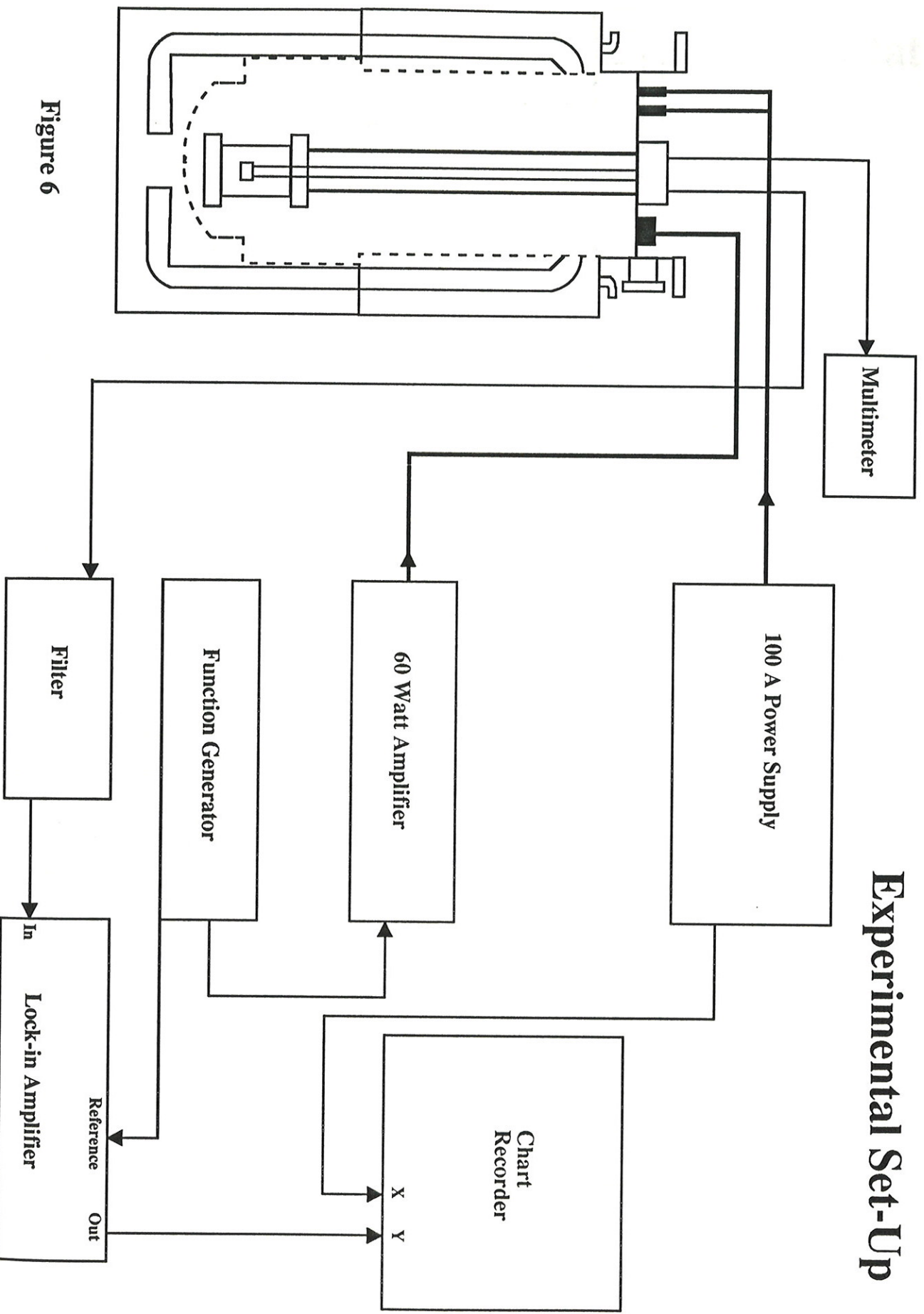


Figure 6

Cryostat

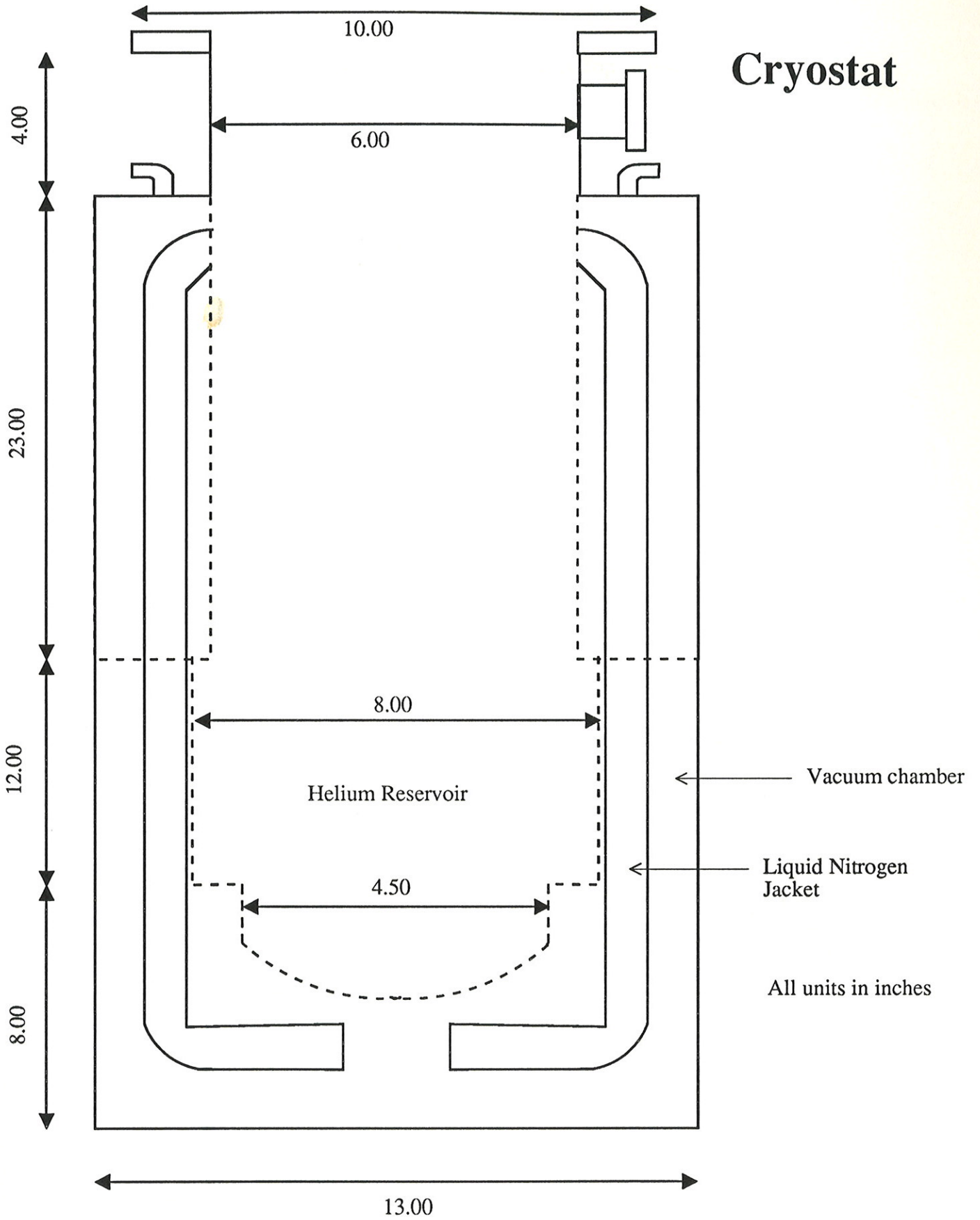


Figure 7 a

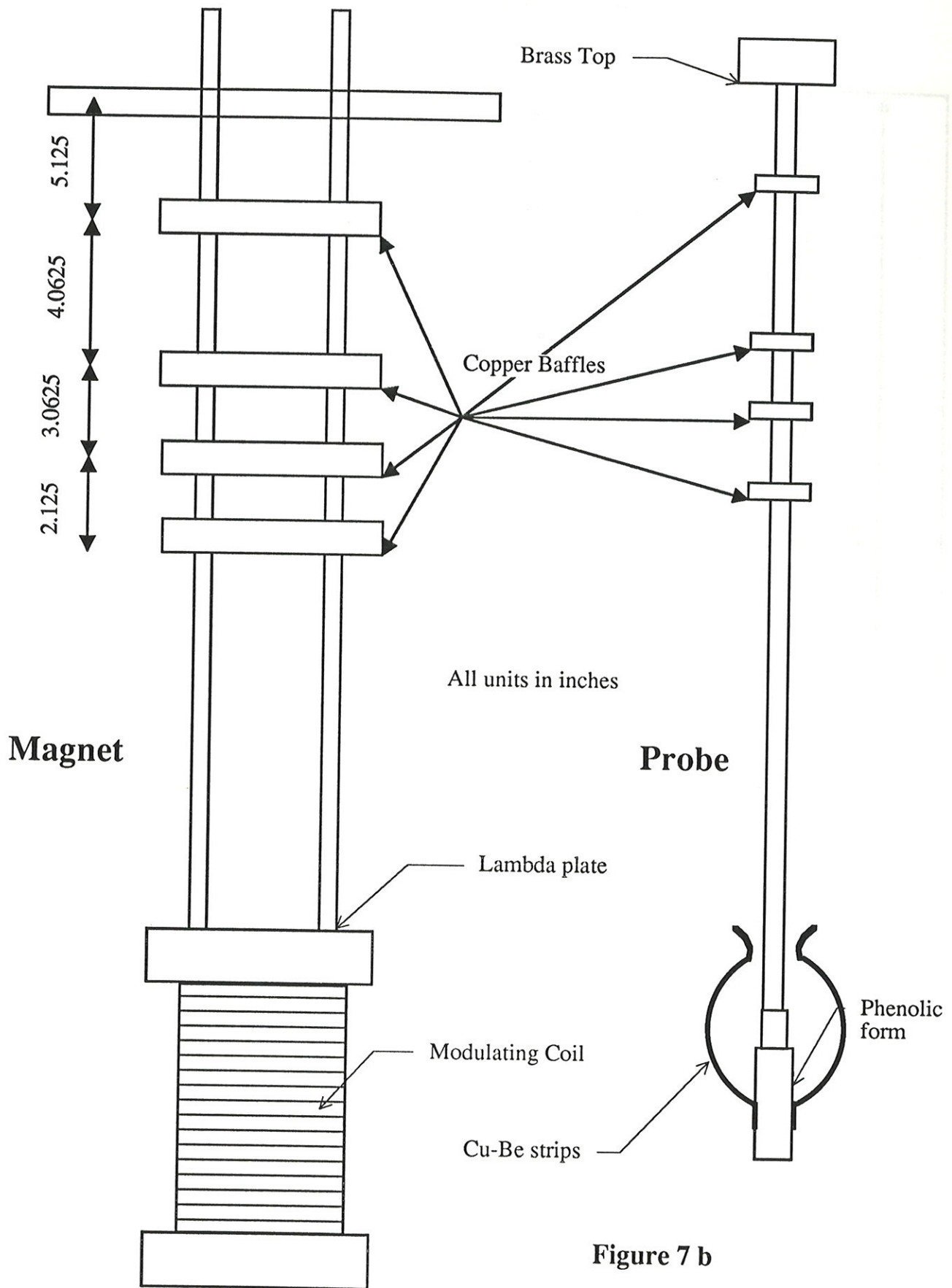


Figure 7 b

Magnet Coils

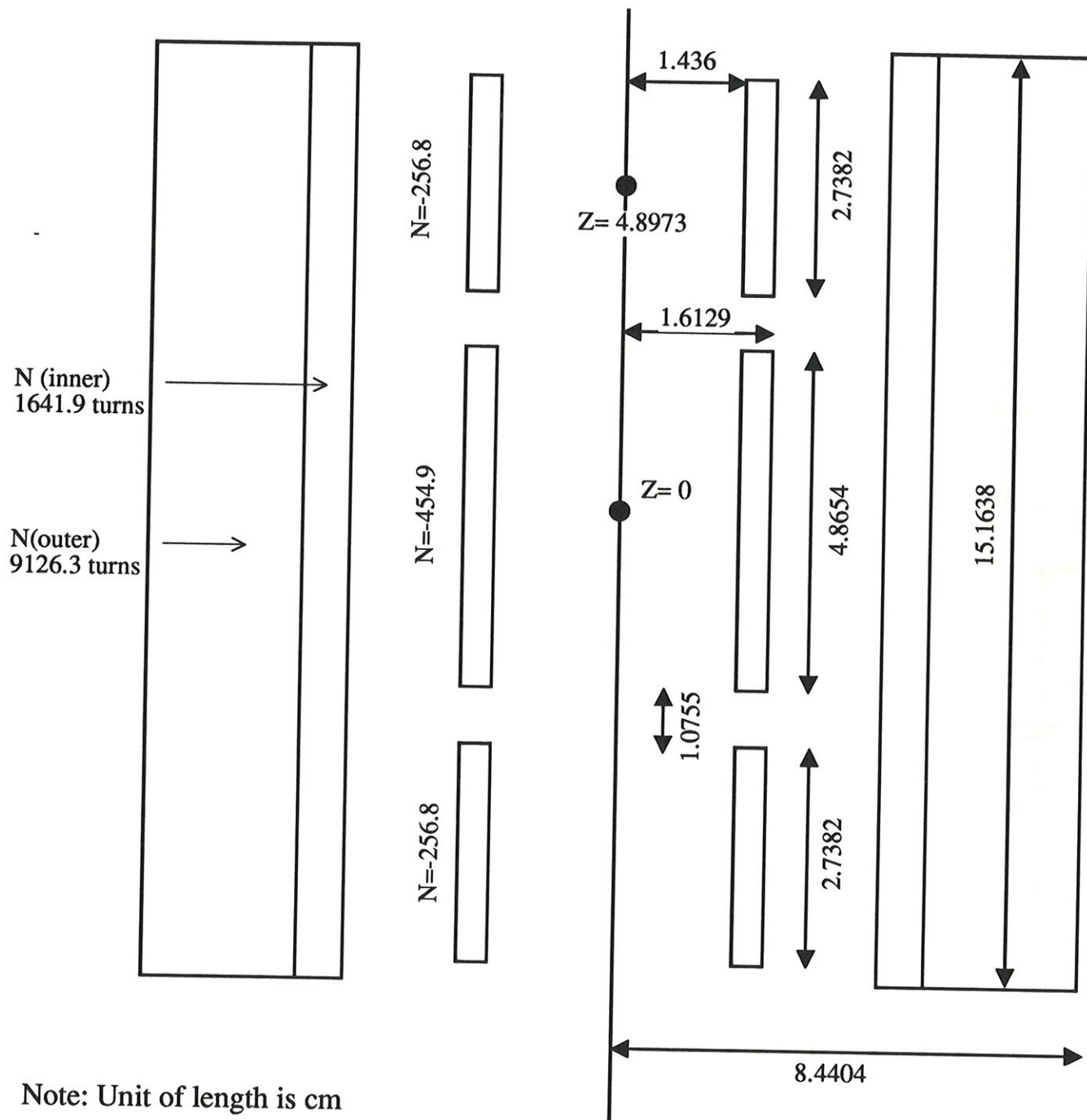


Figure 8

GEAR BOX

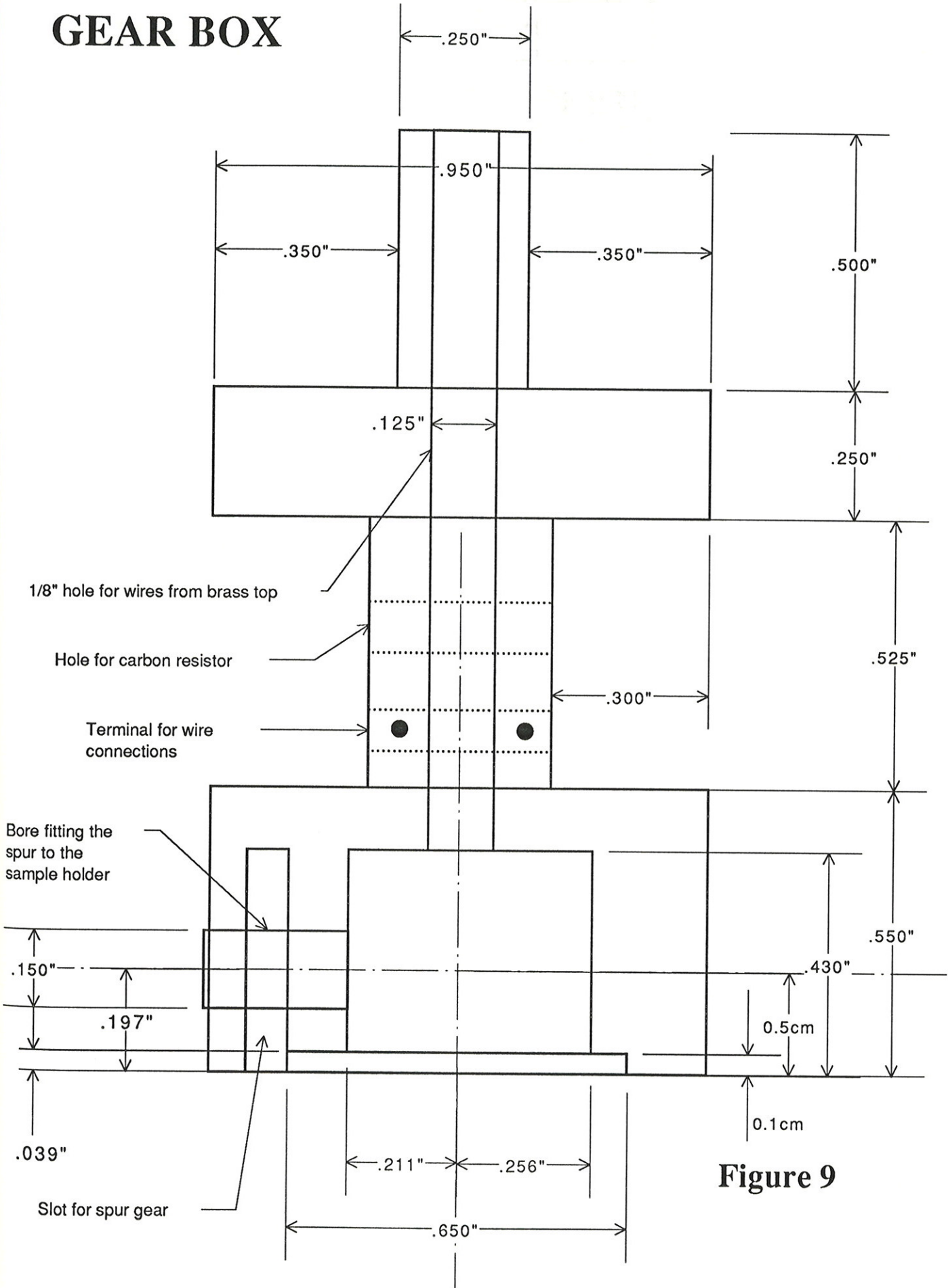


Figure 9

COIL FORM

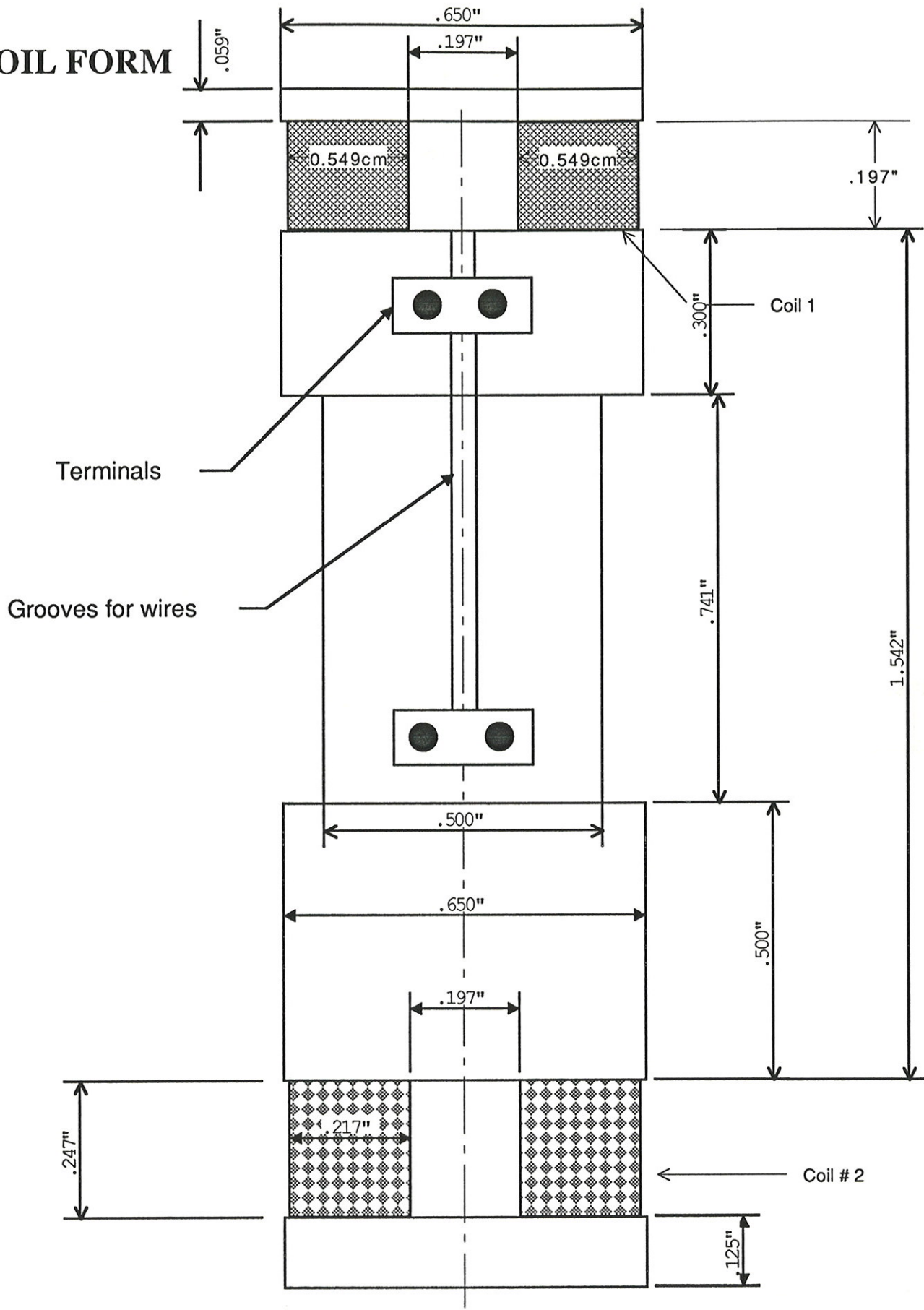
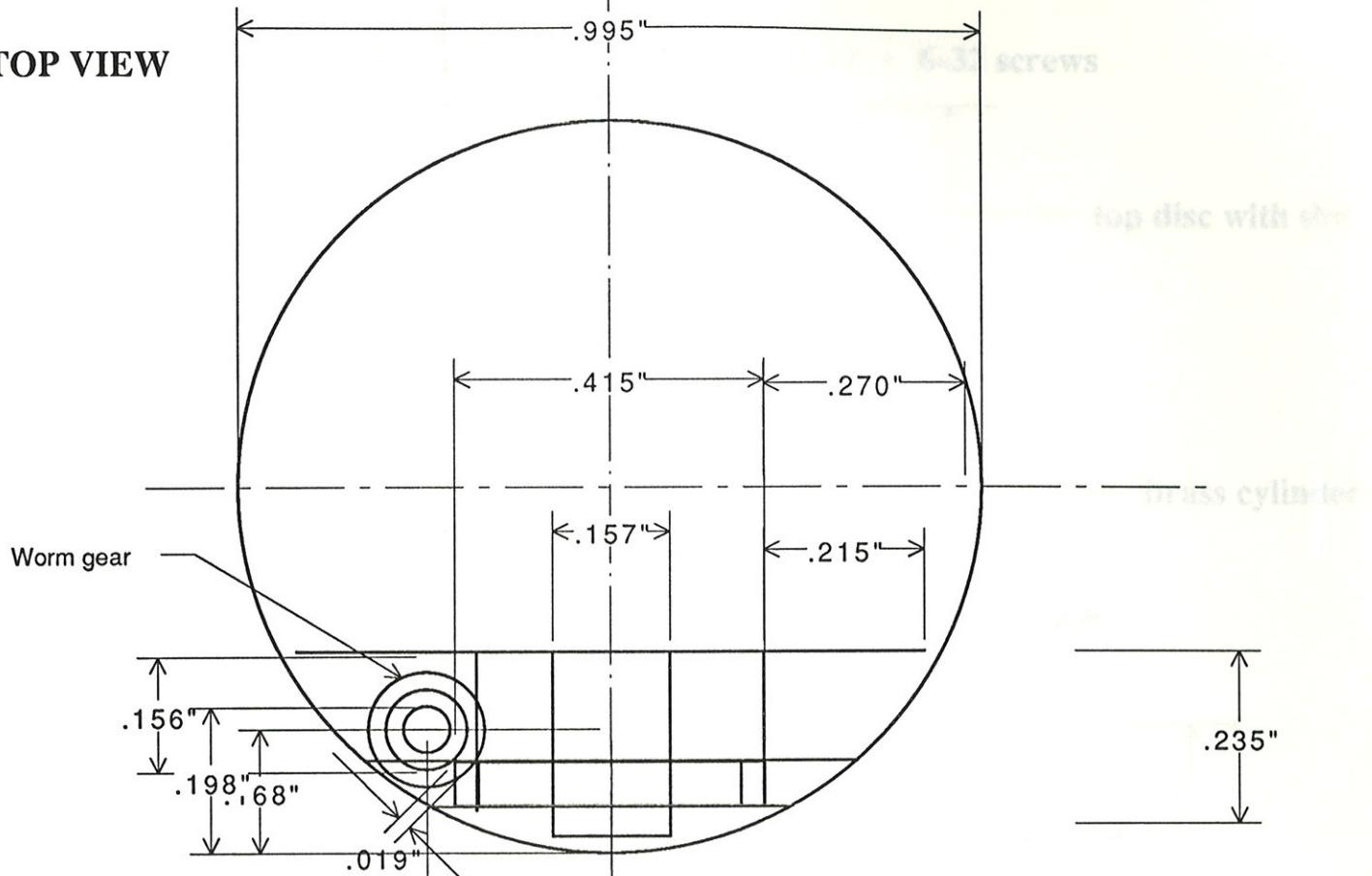


Figure 10

TOP VIEW



SIDE VIEW

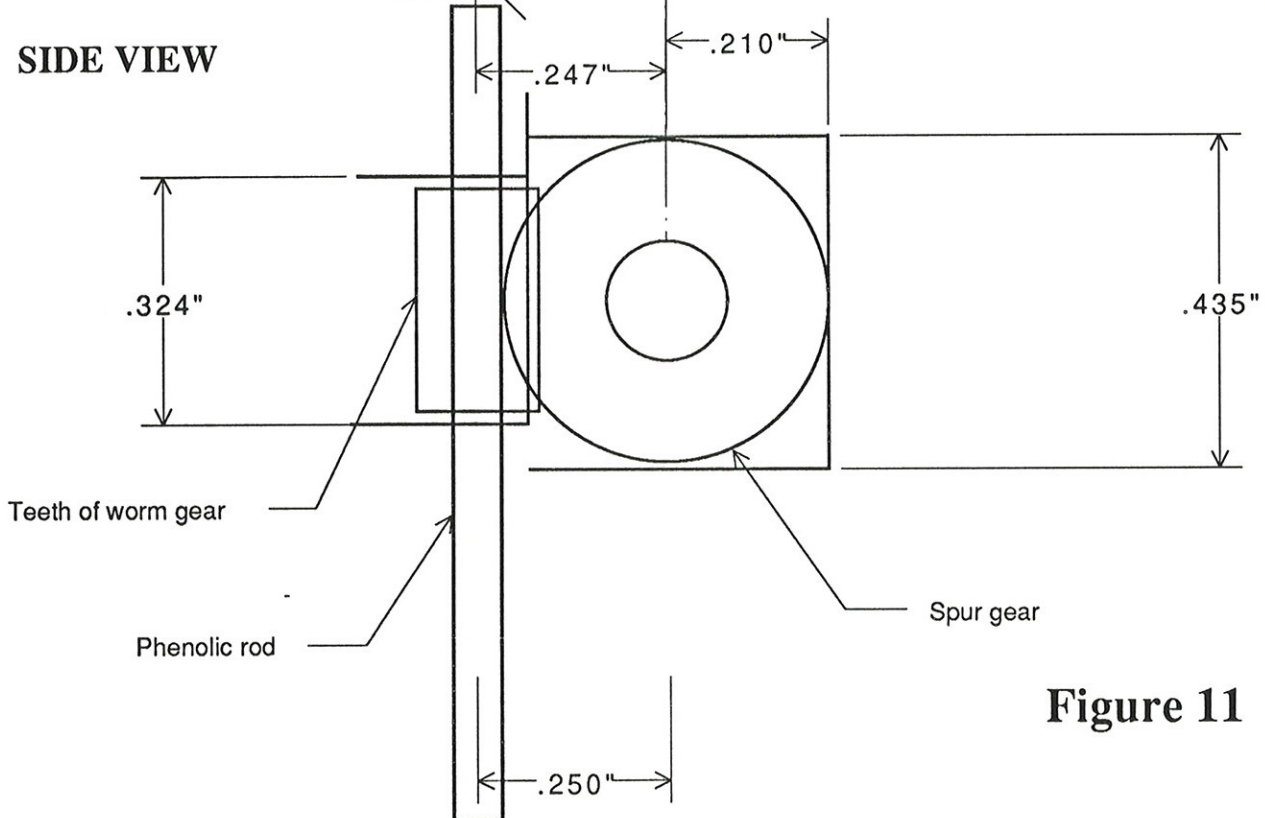


Figure 11

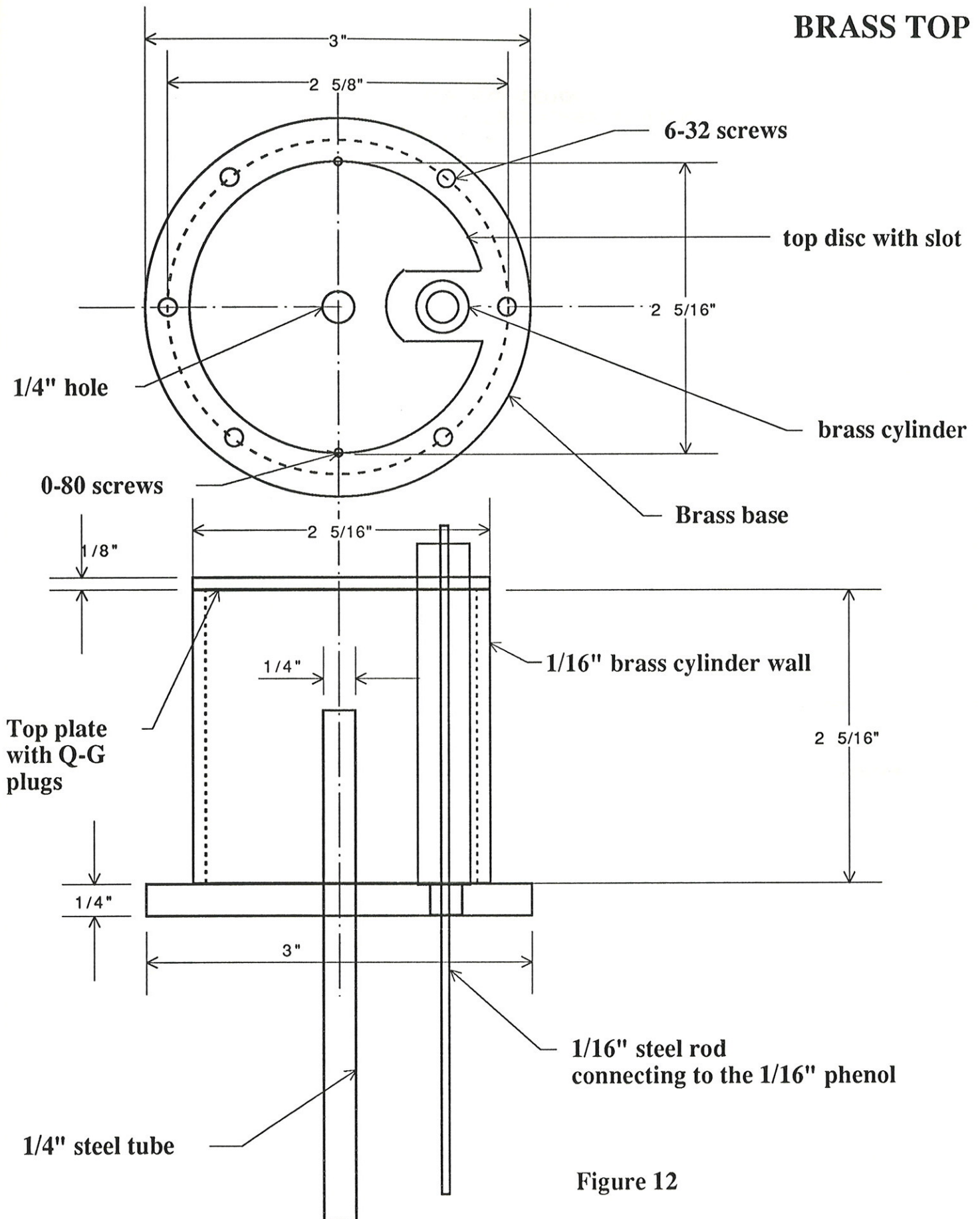


Figure 12

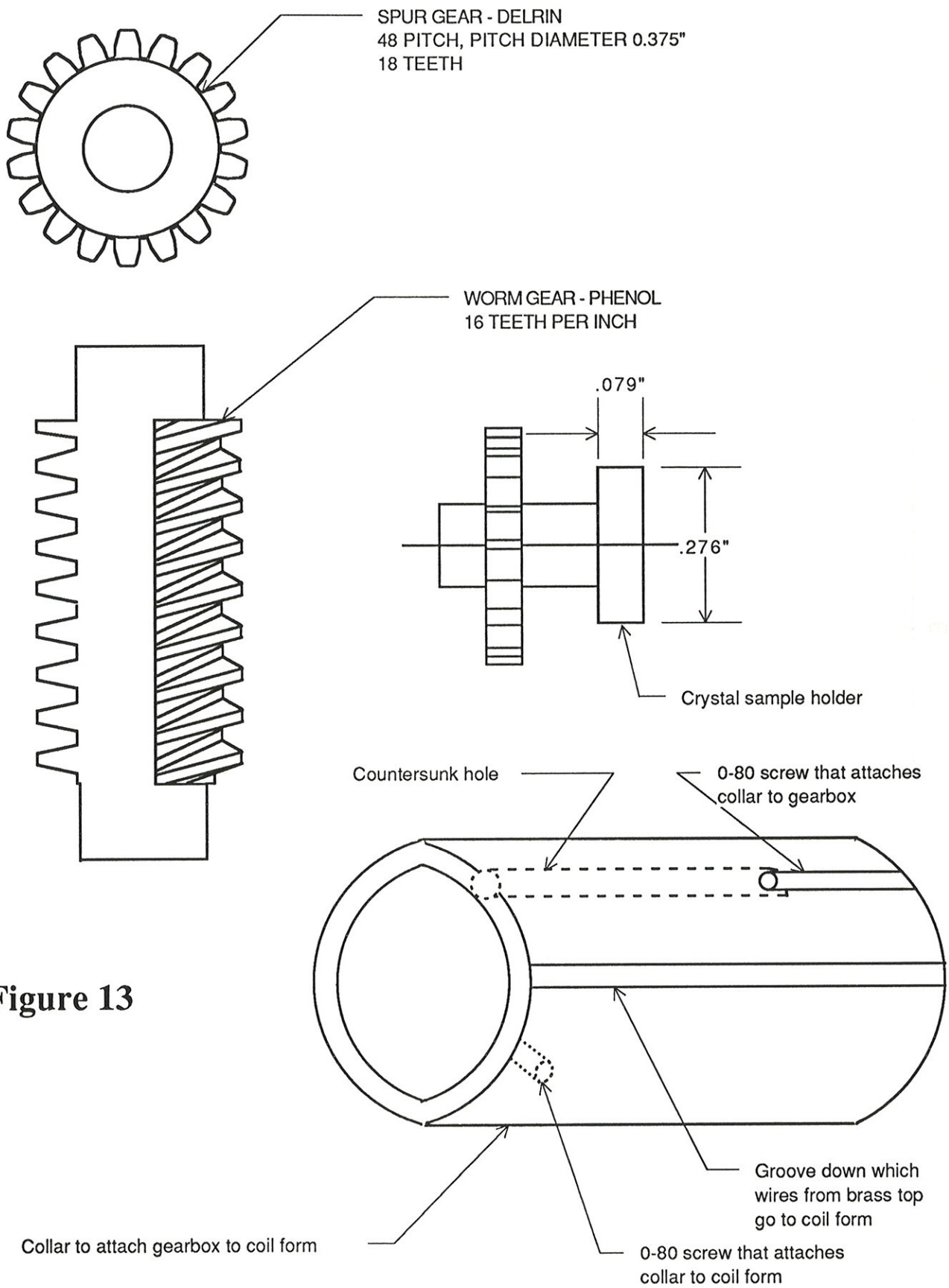


Figure 13

Figure 14
Chart Plot for 120 deg

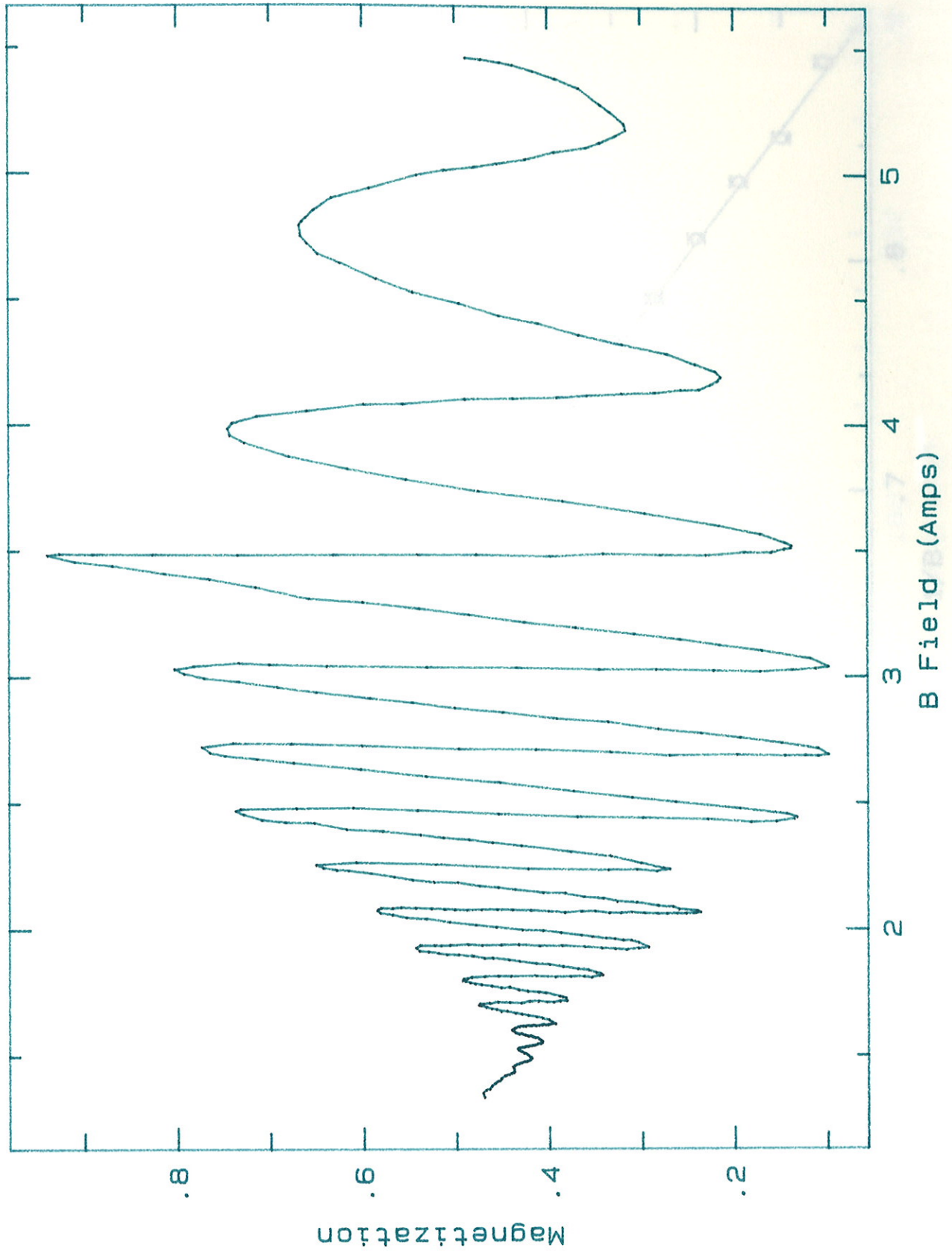


Figure 15
Peak no vs. $1/B$

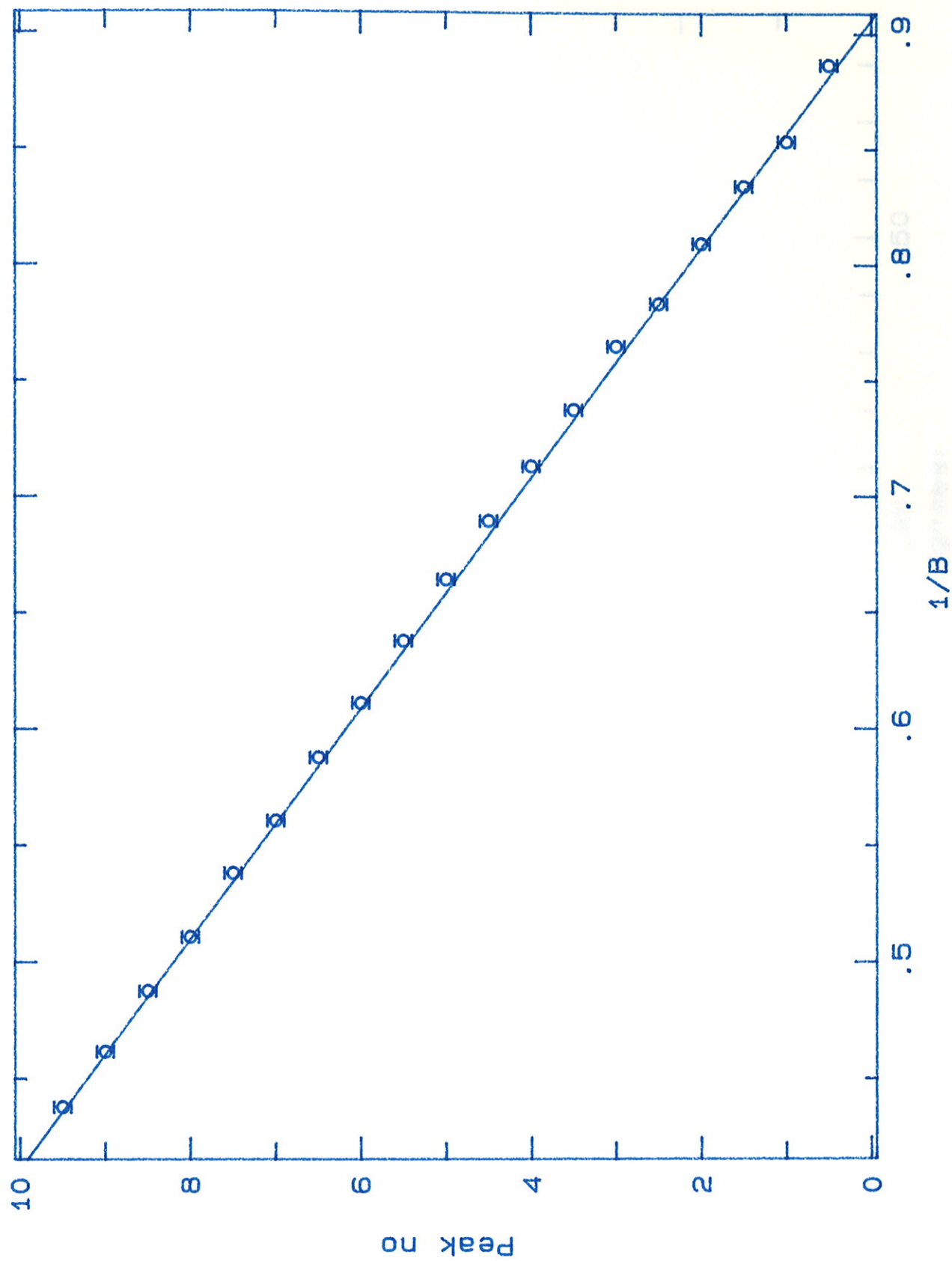


Figure 16
Data w/o Zero Calibration

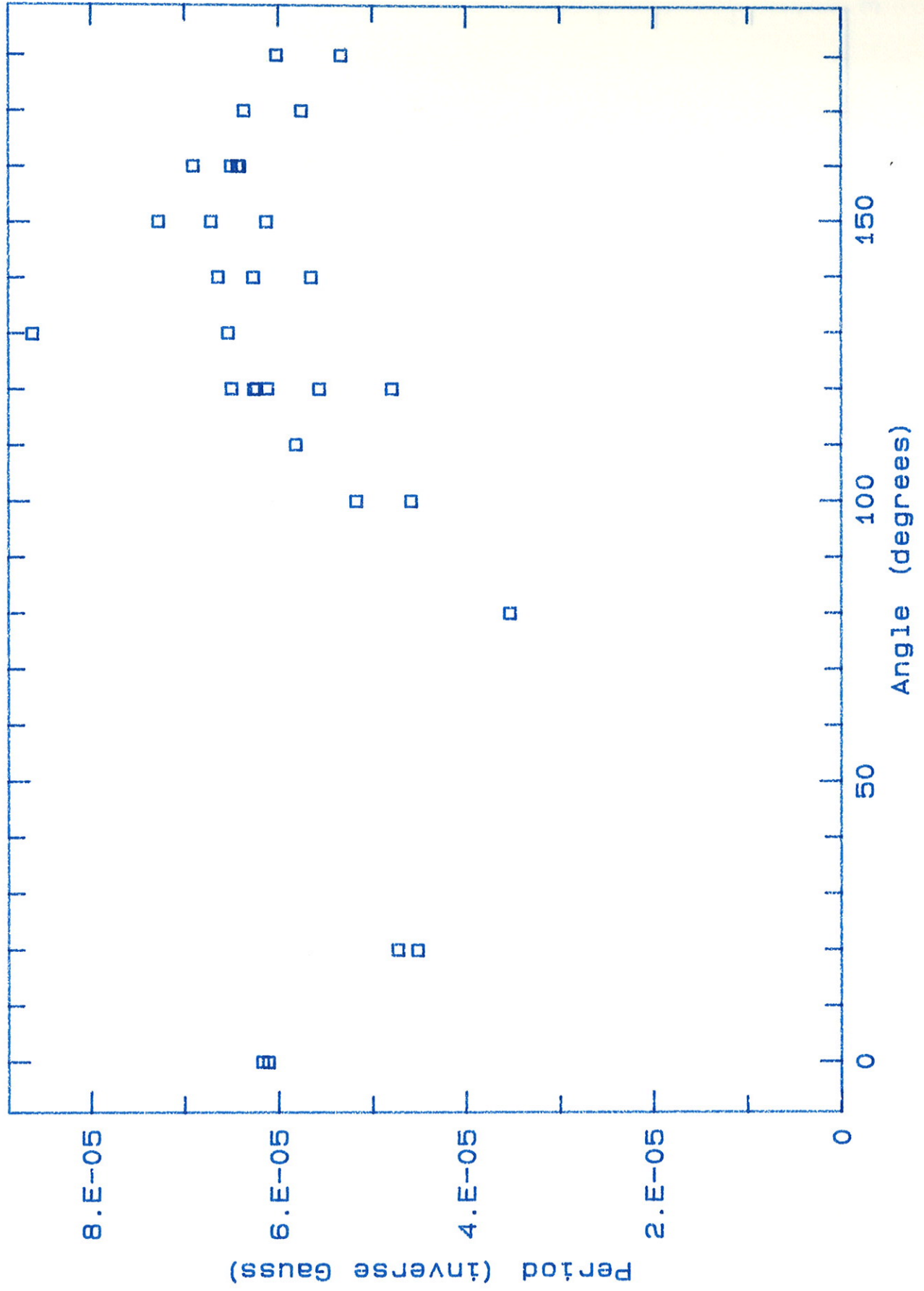


Figure 17
Data w/ Zero Calibration

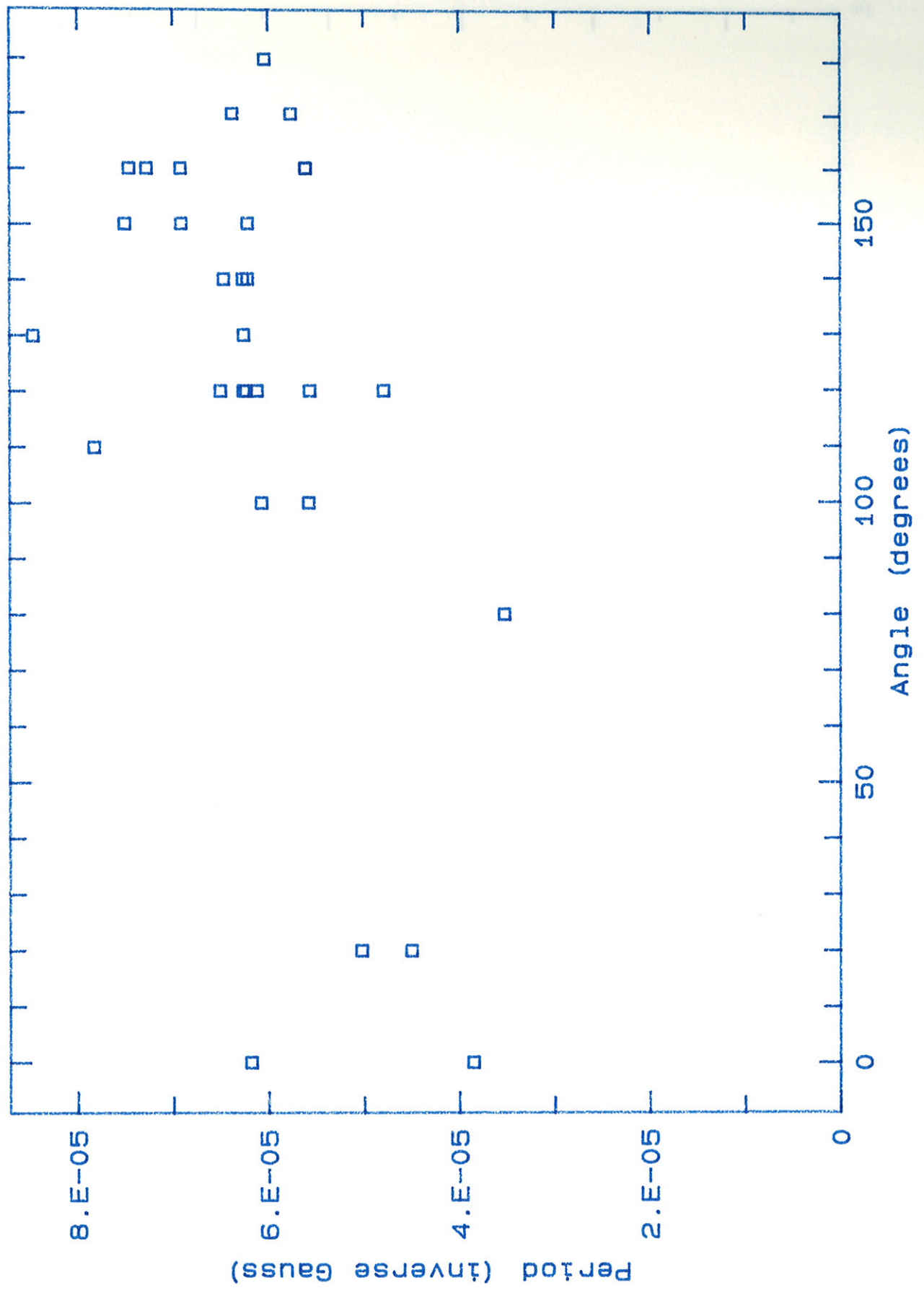


Figure 18
Beats at 130 deg

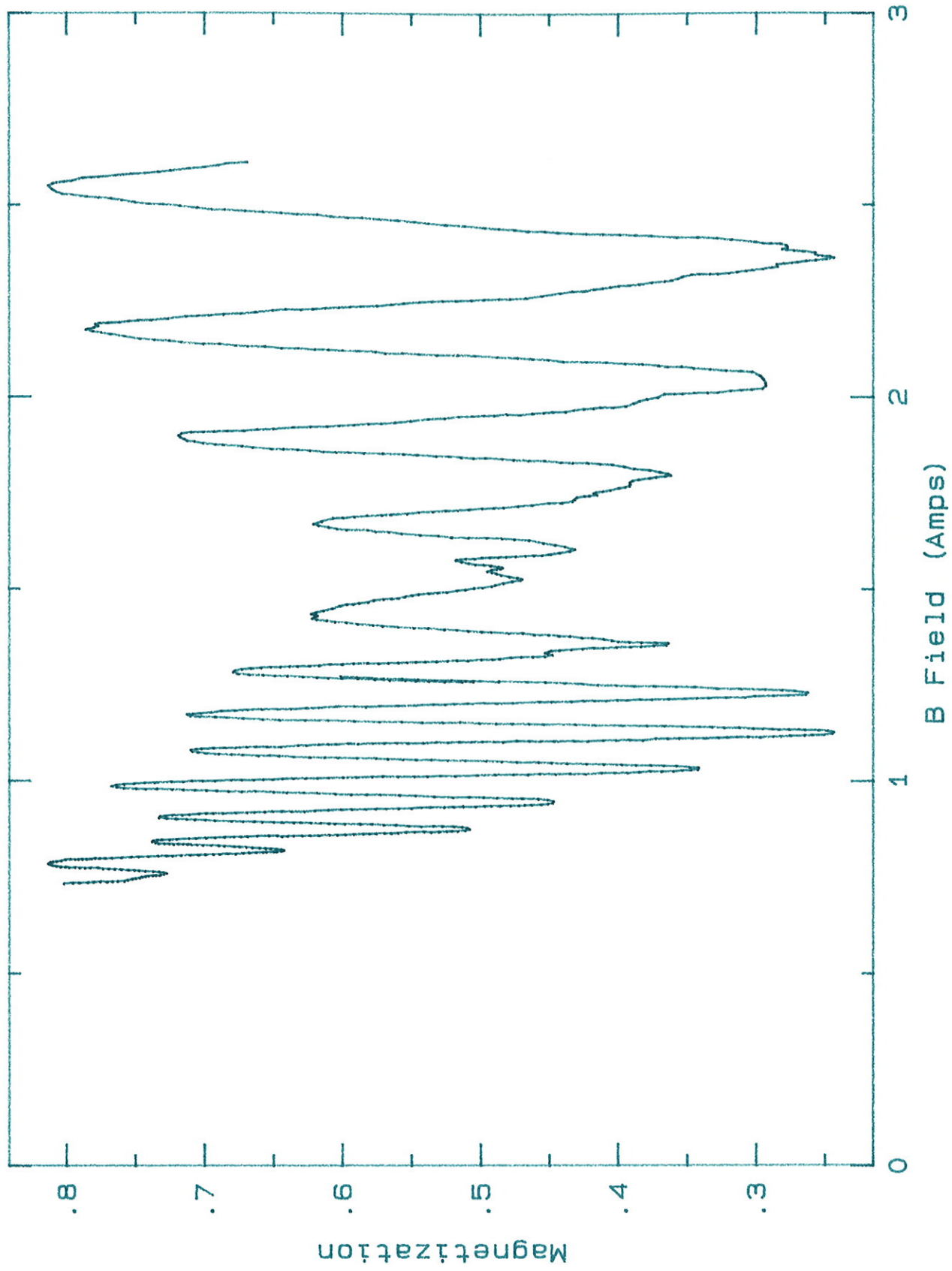


Figure 19
DHVA --- Comparison

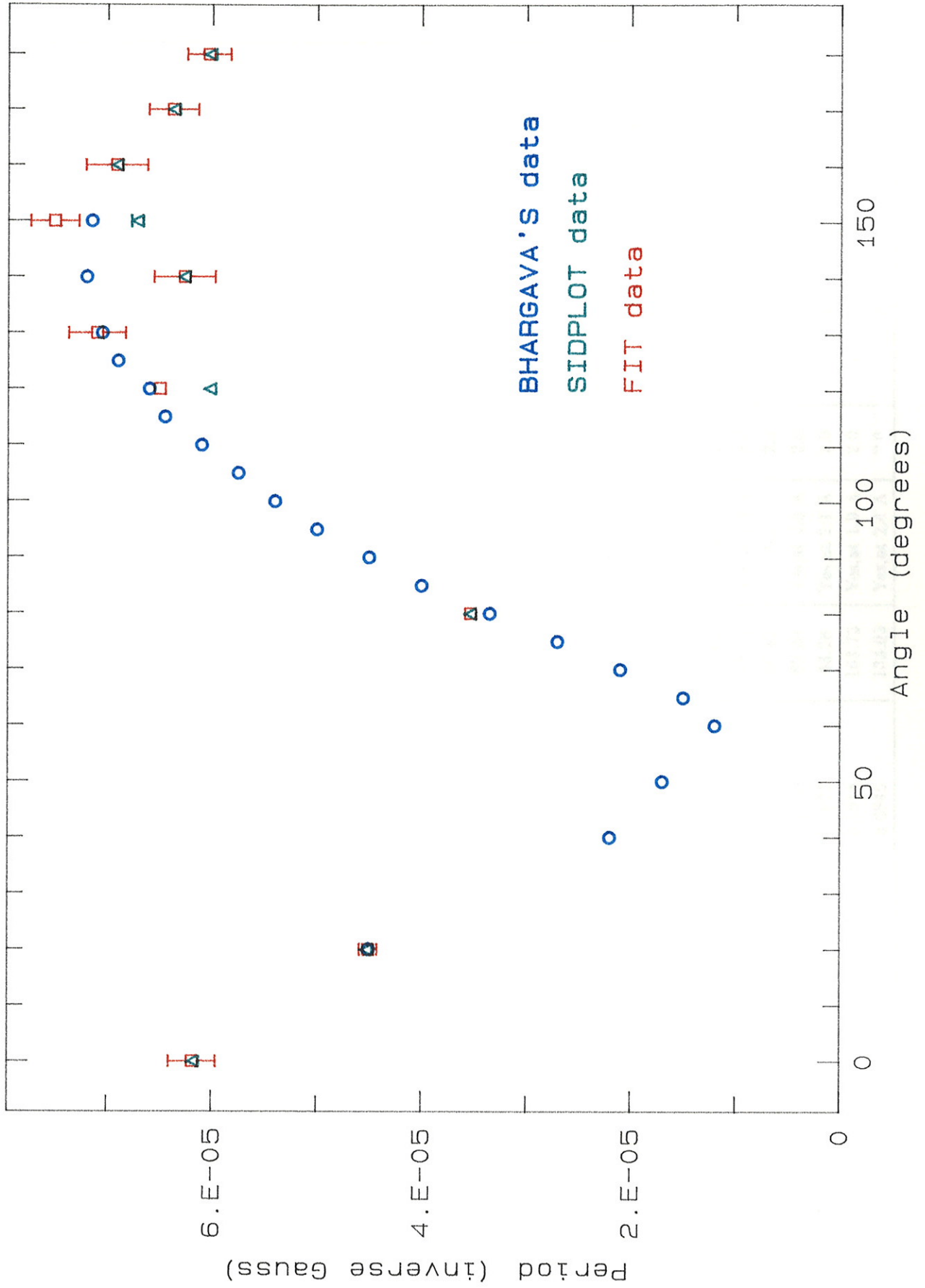


Table 2.

Angle (deg)	Unfitted Period ($\times 10^{-5} G^{-1}$)	Fitted Period w/ ΔB ($\times 10^{-5} G^{-1}$)	ΔB (G)	T ($^{\circ}K$)	Beats	Time constant (sec) Lock-in Amplifier	X-scale (mV) Chart plot
0	6.1095	3.8552	423.28	No	4.2	3.0	25.0
20	4.5197	4.5055	3.70	?	4.2	3.0	25.0
80	3.5343	3.5344	4.38	No	4.2	3.0	25.0
100	4.5879	5.5776	150.02	Yes, at 2.2 A	4.2	3.0	25.0
120	6.7544	5.5670	115.15	No	4.2	3.0	25.0
120	5.0658	6.1170	127.84	No	4.2	3.0	25.0
140	6.2670	6.2658	0.90	?	4.2	3.0	25.0
160	6.4328	7.2957	78.90	Yes, at 2.3 A	4.2	3.0	25.0
160	6.5016	7.4603	88.96	Yes, at 2.3 A	4.2	1.0	25.0
110	5.8172	7.8239	197.97	No	4.2	1.0	25.0
120	5.0658	6.2330	63.02	No	4.2	1.0	25.0
130	6.5365	5.4652	159.67	No	4.2	1.0	25.0
150	6.7171	7.5056	66.96	No	4.2	1.0	25.0
150	7.2802	6.2166	60.42	No	4.2	1.0	25.0
170	6.3654	6.3744	1.54	Yes, at 2.0 A	4.2	1.0	25.0
120	6.0188	6.5010	46.49	No	4.2	1.0	25.0
140	6.6437	6.4671	16.66	Yes, at 2.5 A	4.2	1.0	25.0
160	6.9079	6.9150	1.16	Yes, at 2.2 A	4.2	1.0	25.0
180	6.0188	6.0363	1.15	Yes, at 2.6 A	4.2	1.0	25.0
0	6.1716	6.1831	0.67	Yes, at 2.3 A	4.2	1.0	25.0
20	4.7307	5.0265	49.35	No	4.2	1.0	25.0
100	5.1736	6.0720	119.18	Yes, at 2.0 A	4.2	1.0	25.0
120	5.2632	6.2590	98.85	No	2.0	0.30	25.0
120	5.3091	4.7920	86.65	No	2.0	0.30	10.0
130	9.9380	7.1008	15.44	Yes, at 1.4 A	2.0	0.30	10.0
140	5.6549	6.2166	60.42	No	2.0	0.30	10.0
150	6.2350	7.1250	82.00	Yes, at 2.3 A	2.0	0.30	10.0
160	6.4124	5.6677	63.28	Yes, at 2.1 A	2.0	0.30	10.0
170	5.7566	5.7618	163.73	Yes, at 1.9 A	2.0	0.30	10.0
180	5.3324	5.0849	133.03	Yes, at 2.4 A	2.0	0.30	10.0